UCLA
UCLA Previously Published Works

Title

Multiwavelength High-Detectivity MoS2 Photodetectors with Schottky Contacts

Permalink

https://escholarship.org/uc/item/0sm9b0tr

Journal

ACS Nano, 16(12)

ISSN

1936-0851

Authors

Sun, Yanxiao
Jiang, Luyue
Wang, Zhe
et al.

Publication Date

2022-12-27

DOI

10.1021/acsnano.2c06062

Peer reviewed

eScholarship.org Powered by the California Digital Library
University of California

1 DOI: 10.1002/ ((please add manuscript number))

2 **Article type: Review**

3

4

5 Photodetectors Based on Hybrid Systems Combining Two-dimensional materials and

6 Ferroelectrics

7

8 *Yanxiao Sun*[1], *Gang Niu*[1]*, *Wei Ren*[1], *Xiangjian Meng*[2], *Jinyan Zhao*[1], *Wenbo Luo*[3], *Zuo-*

9 *Guang Ye*[4], *Ya-Hong Xie*[5]

10

11 1. Electronic Materials Research Laboratory, Key Laboratory of the Ministry of

12 Education & International Center for Dielectric Research, School of Electronic Science

13 and Engineering, Xi'an Jiaotong University, No. 28, Xianning West Road, Xi'an, Shaanxi,

14 710049, P.R. China

15 E-mail: gangniu@xjtu.edu.cn

16 2. National Laboratory for Infrared Physics, Shanghai Institute of Technical Physics,

17 Chinese Academy of Sciences, Shanghai, China

18 3. State Key Laboratory of Electronic Thin Films and Integrated Devices, University of

19 Electronic Science and Technology of China, Chengdu, 611731 China

20 4. Department of Chemistry and 4D LABS, Simon Fraser University, Burnaby, British

21 Columbia, V5A 1S6, Canada

22 5. Department of Materials Science and Engineering, University of California, Los

23 Angeles, Los Angeles, California, United States

24

25 Keywords: two-dimensional materials; ferroelectrics; photodetectors; hybrid systems

26

Two-dimensional materials have been extensively studied in last decades due to their remarkable physical, electrical and optoelectronic properties. Meanwhile, combination of two-dimensional materials with traditional functional materials have provided new approach in a variety of research and application areas. In this review, we have focused on the two-dimensional and ferroelectric hybrid system being applied in photodetection. Fundamentals of the materials and interaction in the hybrid system was introduced. Modulation of the optoelectronic properties induced by ferroelectricity was discussed in the hybrid system. After introducing the basics of photodetection, the devices were categorized and reviewed based on their structures. Modulation and enhancement of the photodetectors were observed with ferroelectric polarization. Finally, the challenges and perspectives of the photodetectors based on two-dimensional materials and ferroelectrics have been proposed.

1. Introduction

Last decades have witnessed rapid development of photonic and optoelectronic devices which demonstrate a wide spectrum of applications including photo-emission (eg. photodiodes[1, 2, 3, 4], LEDs[5, 6] and lasers[7, 8]), photodetection[9, 10, 11, 12, 13], data storage[14, 15] and energy storage[16, 17]. Nowadays, the information society featuring “Internet of Things” and “big data” demands further evolution of electronics and optoelectronics, particularly for telecommunication and communication. Photodetectors, serving as the receiving end, are one of the most important components in such optic communication network. [18] Photodetectors are among the most ubiquitous devices with superiorities of the sufficiently fast response, the high detectivity, the remarkable data storage capability etc. Photodetectors detect light in a certain range of frequency band and the device performance can be evaluated by a series of figures of merit, which are dominated by the device structure and more importantly by detecting materials. Among the massive materials and devices applied in the photodetection, semiconductor-based photodetectors have attracted intense interest from both academic and

53 industrial fields, thanks to their smaller size, wide band detection and Si-technology
54 compatibility. These photodetectors could be tailored by simply altering the composition of
55 the various layers forming the structure. Both individual devices and the component in the
56 communication system requires compact structure, ultra-thin devices and further optimization
57 of the opto-electronic properties, which has triggered the flourishing of novel materials with
58 outstanding structure and properties.
59 Conventional materials applied in electronic and optoelectronic semiconductor devices are
60 crystalline silicon (Si) and germanium (Ge). Compounds of III-V semiconductors such as
61 Gallium (Ga), Indium (In), Arsenic (As), Phosphorus (P) and antimony (Sb) are also applied
62 in the materials as well as the alloys due to their direct bandgap property and have been
63 intensively studied for years.[19, 20, 21] More recently, with the advent of two-dimensional
64 (2D) materials,[22, 23] various new photodetection phenomenon have been reported due to
65 their mechanical, thermal, electrical, optical and optoelectronic properties distinguished from
66 that of the three-dimensional counterparts, [24, 25, 26] which has made a tremendous
67 progress of photodetectors. Materials with Van der Waals bonds interlayers usually form thick
68 bulk or crystals which makes them difficult utilized in nanodevices. Such obstacle was
69 overcome by the Novoselov and Geim in 2004, who successfully exfoliated the graphene
70 nano flake and applied it in a field-effect transistor (FET) for ultrafast photodetection.[27, 28]
71 Since then, 2D materials have rapidly been established as building blocks for photodetectors
72 due to their remarkable optical and optoelectronic properties.[29, 30, 31] Fabrication
73 procedure of 2D materials photodetectors is quite simple, which as well provides a facile
74 platform for micro- and nano- devices fabrication.[32, 33] In general, 2D materials are
75 potential in building highly integrated and efficient photodetectors, and promising candidate
76 for the future integrated optoelectronic devices as well.
77 The library of 2D materials has experienced a gradual expansion from graphene to its
78 derivatives (eg. graphene, carbon nano tubes (CNTs), hexagonal boron nitride (h-BN), and to

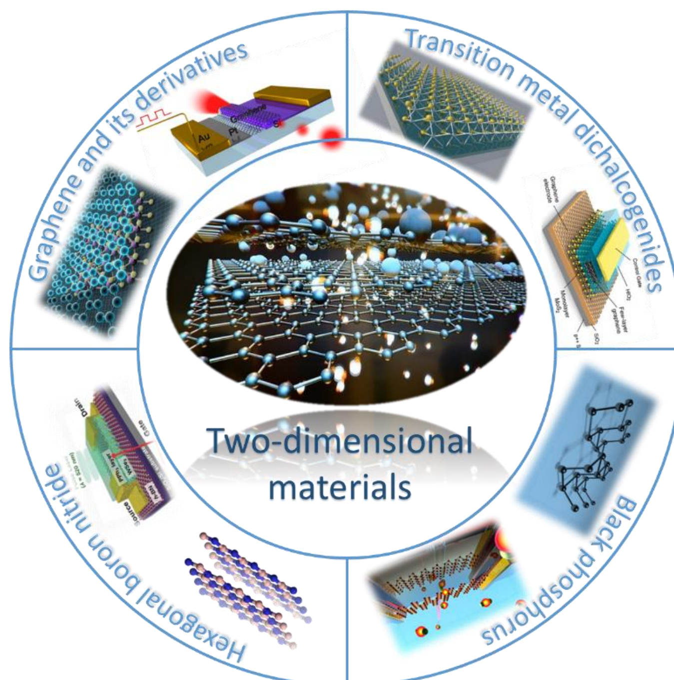

Figure 1. Categories of 2D materials and their applications in electronics and optoelectronics. [34, 35, 36] Copyright Year, Publisher.

layered group-IV and group-III metal chalcogenides, as well as to layered transition metal dichalcogenides (TMDs) with their alloys and heterostructures and other novel functional materials etc., as summarized in Figure 1.[34, 35, 36] With the growth of 2D materials family, they have covered from metal, semiconductor to insulators now. 2D materials have ultra-thin physical structure ranging from ~0.4 nm (one monolayer) to bulk materials with tens of nanometers. Some 2D materials, like graphene and TMDs, show a typical bandgap transition with the thickness variation, which provide opportunities for bandgap modulation. [37] Meanwhile, Electrical and optoelectronic properties of the 2D materials are closely related to the band structure, which corresponding to the thickness variation and bandgap modulation in 2D materials.[38] Furthermore, The atomic-scale thickness of 2D materials leads to the high transparency and flexibility, which is of particular interest in novel wearable, flexible and portable devices.

94 Meanwhile, another category of materials being employed in electronic and optoelectronic
95 devices are functional materials, also known as "smart materials", with typical properties
96 responding to the external stimuli. [39] Functional materials are capable of coupling the input
97 (eg. electric field, magnetic field, stress, light field and heat) and output (eg. charge/current,
98 magnetization, strain, light and temperature), as shown in Figure 2.[40] The "smart materials"
99 nowadays are widely applied in actuators, sensors and detectors. Among smart materials,
100 ferroelectrics is unique due to its spontaneous reversal of polarization with switching of
101 external electric field. Main application areas of ferroelectrics include energy harvesting,
102 memory devices and data storage devices.[41, 42, 43, 44]. More and more electronic devices
103 and photodetectors with profound performances are achieved with ferroelectric materials
104 employed. [45]

105 Photodetection could be realized with ferroelectrics as active layers, where polarization of the
106 materials could be altered by the incident light, resulted in linear, nonlinear optical or
107 electrical output. Furthermore, polarization of the ferroelectrics enables wavelengths
108 modulation by altering of the applied polarization direction. Both inorganic ferroelectric
109 materials like $Pb(Zr,Ti)O_3$ (PZT),[46, 47, 48, 49] $BaTiO_3$ (BTO),[50, 51] $LiNbO_3$ (LN),[52,
110 53] $BiFeO_3$ (BFO)[54, 55, 56] and organic compounds PVDF as well as the derivatives[57,
111 58]have been studied and applied in photodetectors. Nevertheless, ferroelectrics can only
112 response to limited frequency band width of light, for other incident light to which
113 ferroelectrics are unable to response, other group of the materials could be introduced. 2D
114 materials, which are known for their wide band response could combine with ferroelectric
115 layers. Such hybrid photodetection systems might probably lead to new phenomena and
116 therefore become a topic attracting increasing studies. As for the photodetectors, the hybrid
117 structure could modulate the carriers and performance of the devices could be optimized.

118 In addition to the materials chosen in photodetection, structure of the devices is also of vital
119 importance. Grouped by structures, photodetectors include devices like phototubes,

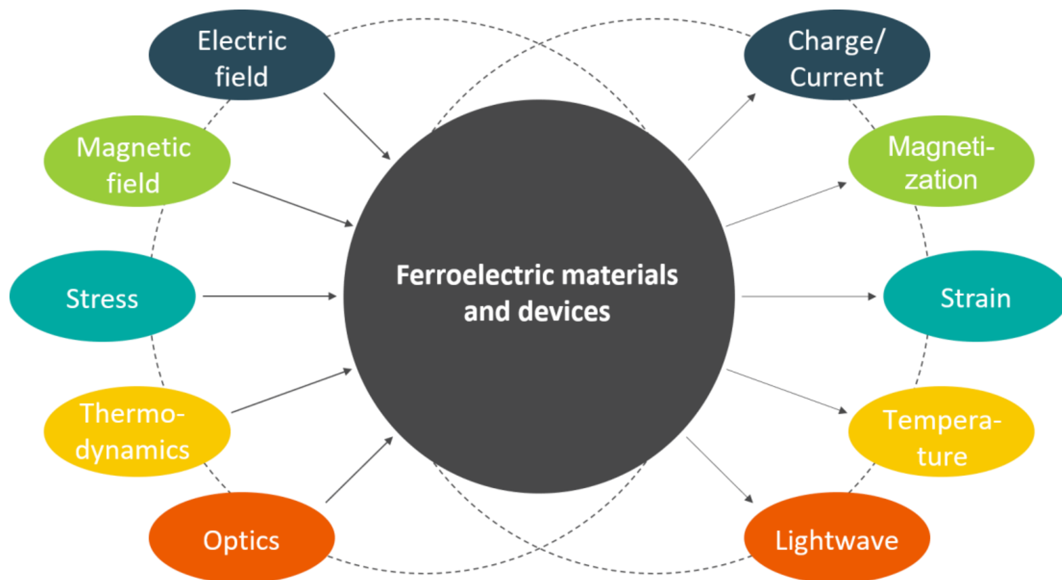

120

121 **Figure 2.** Coupling of the fields in ferroelectric materials and devices

122 photomultipliers and semiconductor photodetectors. Phototubes and photomultipliers are
123 mostly applied as dependent devices. As for the semiconductor photodetectors, one of the
124 most prominent advantages is its capability of been compacted into integrated circuits.
125 Furthermore, photodetection arrays could thus been achieved. Basic structures of the
126 semiconductor photodetectors could be categorized into PN diodes, Schottky diodes as well as
127 field effect transistors *etc.*.

128 In this work, we review the structures and devices based on ferroelectrics and 2D materials
129 hybrid system for photodetection. Fundamentals of the 2D materials and ferroelectrics
130 including structure, electrical, optoelectronic and interaction of the hybrid system are
131 presented. After that, various structures and corresponding nano devices for photodetection
132 are discussed in detail, including PN junctions, field effect transistors and other types of
133 devices. Performances of the hybrid devices was summarized and discussed. This review
134 outlines the important aspects of the ferroelectrics-2D materials hybrid photodetectors and is
135 certainly of great interest for design novel photodetectors.

136 **2. Fundamentals of 2D materials and ferroelectrics**

137 **2.1. Fundamentals of 2D materials**

138 Exfoliation of the monolayer graphene has opened the door to research 2D materials.
139 Monolayer graphene was applied in the FET and the outstanding electrical and structure
140 property were observed. With deep exploration of graphene and its relative derives, as well as
141 other 2D materials with similar structure for instance the hexagonal-boron nitride (h-BN),
142 TMDs and black phosphorus (BP). These novel 2D materials share excellent optical and
143 optoelectronic properties, which attracting more research for optoelectronic devices.

144 2.1.1. Graphene

145 It was convinced that nano-materials were hardly remain stable due to thermal fluctuation,
146 which consequently lead to decomposition of the materials. In this case, the thermally stable
147 and chemically inert graphene has brought big surprise to scientist, leading to booming
148 development of 2D materials research area in the past decades.[33, 59, 60] Researchers tried
149 to add the "fresh blood" into the "old fashioned" methods, devices and systems to create
150 novel structures and to improve the performance.

151 Graphene has in-plane chemistry bond connecting the atoms and can stack with Van der
152 Waals forces between layers. The structure of graphene is hexagonal arrangement of sp^2-
153 bonded carbon atoms with zero bandgap and Dirac point. In graphene, single layer of carbon
154 atoms with sp^2-hybridization arranged in a honeycomb lattice, which is just one atom thick at
155 vertical dimension (about 0.14 nm). Each carbon atom in-plane bonds to other three nearest
156 atoms with a distance of 1.42 Å, shown in Figure 3.[61] The lattice of graphene can be
157 considered as two interpenetrating triangular sub-lattice A and B, see in Figure 4(a). Band
158 structure in graphene materials could be modeled by the tight-binding approximation as well
159 as calculated based on the first principle.[62, 63, 64], as shown in Figure 4(b) and (c).

160 The p_z orbitals remained, which do not involve in the covalent bonding, is responsible for the
161 electric conductivity. Graphene is a promising candidate for electronic devices with
162 outstanding electrical properties. Conductivity and mobility of the graphene nanosheets

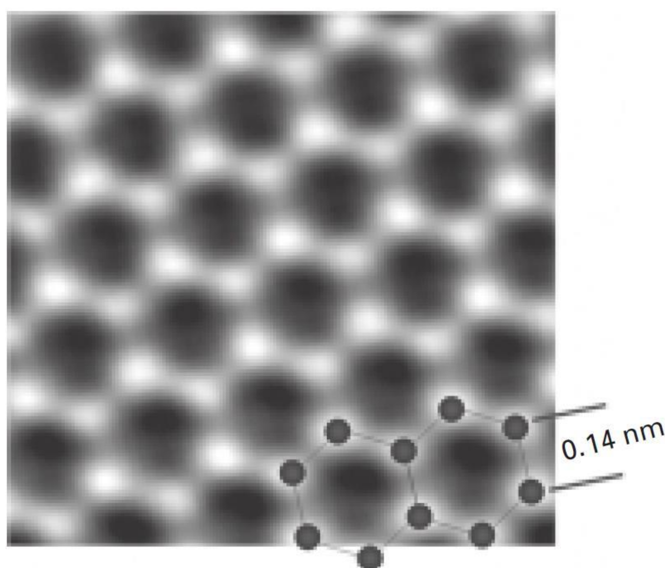

163

164 **Figure 3.** Atomic structure of graphene nanosheets demonstrated the bond between the atoms
165 and the honeycomb structure of the graphene layer (courtesy of Berkeley's TEAM05, 2009).

166 mostly depend on the defect scattering process, which is almost independent from temperature.
167 [65] The minimum conductivity of graphene theoretically exhibits at the Dirac point as
168 $4e^2/\pi h$. The electron mobility ranges from ~0.67×10^4 $cm^2V^{-1}s^{-1}$ up to 10^6 $cm^2V^{-1}s^{-1}$ in the
169 form of suspended nanosheets or supported by SiO_2/Si substrates. [30, 66, 67] Meanwhile,
170 high current carrying capacity of ~5.8×10^6 $A\cdot cm^{-2}$ and ~1.8×10^9 $A\cdot cm^{-2}$ in graphene/Cu nano-
171 composite wires and on synthetic diamond substrate, respectively.[68, 69, 70] Such high
172 current carrying capacity is particularly feasible for the energy storage system and device
173 minimization. Additionally, high thermal conductivity ranging from ~4840 W/m·K to 5300
174 W/m·K has been observed in layered graphene nanosheets, indicating their outstanding heat
175 dissipation capability, which can be beneficial for batteries and thermal conductive devices.
176 [71]Relative low contact resistance 100 Ω·μm between graphene and metal electrodes allows
177 the application of electronic devices with low Schottky barrier height.[72] Graphene is
178 different from conventional metals not only due to its 2D structure and transparency in a wide
179 band incident light but also because of its ambipolar field effect transport property. Graphene
180 is consequently known as the "semimetal".[73, 74, 75, 76, 77, 78]

181
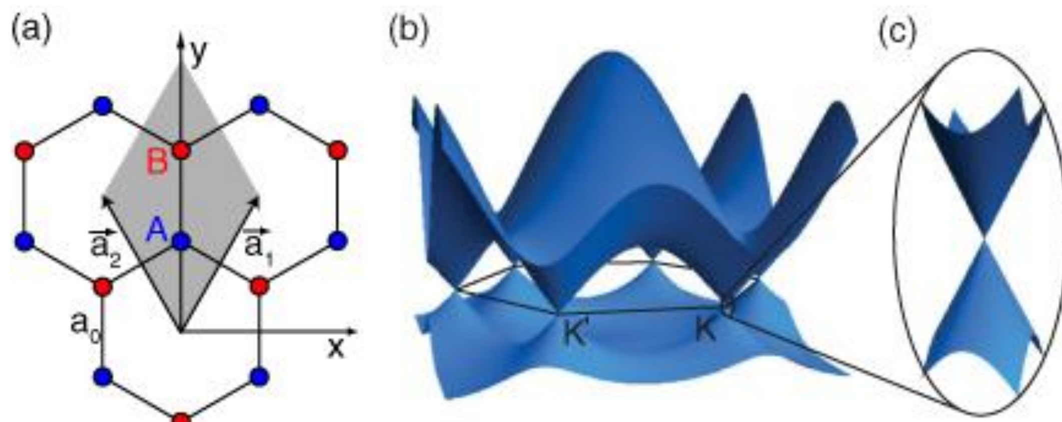

182 **Figure 4.** (a) lattice, (b) band structure and (c) zero-bandgap achieved by tight-binding
183 approximation

184 As the zero-band gap structure, graphene should theoretically be capable of responding to all
185 the photons, which consequently leads to the advantage of wide band detection from
186 ultraviolet to infra-red and all the way to Terahertz region.[31, 79, 80] In addition to the wide
187 band response properties, pristine monolayer graphene is of high transparency, with
188 absorption of 2.3% in a wide band. [81] Such high transmittance brings the opportunity for
189 graphene being applied as transparent electrodes, especially for those allow large absorption
190 area. Moreover, broad band absorption of graphene could be modulated by shifting the
191 electronic Fermi level, which could consequently dominate the photon transition in graphene
192 nanosheets.[82, 83] With interaction of incident light, energy could be converted among
193 carriers, photons and phonons in graphene by transition of the charge carriers (electrons and
194 holes). Macroscopic phenomena such as photon absorption,[84, 85] nonlinear optical
195 properties[86, 87, 88], plasmons,[89, 90] and photo-current have been observed.

196 2.1.2. Transition Metal Dichalcogenides

197 Another group of 2D materials with intrinsic bandgap and similar electrical properties, as well
198 as optoelectrical properties with graphene are TMDs. TMDs with chemical formula MX_2, is a
199 group of materials composed of transition metal (eg. Mo, W, etc.) and chalcogen (eg. S, Se,
200 Te, etc.), as shown in Figure 5. TMDs share similar structures that can be categorized into

IVB	VB	VIB	VIIB	VIII				VIA
22 Ti	23 V	24 Cr	25 Mn	26 Fe	27 Co	28 Ni		16 S
40 Zr	41 Nb	42 Mo	43 Tc	44 Ru	45 Rh	46 Pd		34 Se
72 Hf	73 Ta	74 W	75 Re	76 Os	77 Ir	78 Pt		52 Te

Figure 5. Elements for TMDs. The ones marked in orange means only some of the compounds can form int layered structures

several polytypes varying in stacking orders and metal atom coordination, as shown in Figure 6.[91] The 2H, 3R and 1T phases are the most stable and common structure of TMDs, among which 1H is the most stable and the most studied structure. 3R and 1T phase are metastable and can be converted into 2H by annealing, heating or laser excitation. [92, 93] Properties of different compounds varies at conductivity. For example, compounds with M=Mo and W, X=Se and S are semiconducting,[94, 95, 96] while with M=Nb and Ta are metallic.[97] TMDs experience the transition of indirect bandgap to direct optical bandgap with the number of layers decreased to bilayer or monolayer, as shown in Figure 7.[98] The bandgap ranges from 1.0 eV to 2.1 eV, see in Table 1. Some of the TMDs, like TiS_2 and WT_2, show zero bandgap structure, being similar to graphene. Bandgap modulation is desired for applications of TMDs in nano-devices under certain circumstances due to the requirement of tunable electronic properties. Therefore, bandgap modulation by strain engineering, electric field control, alloying and hybrid system fabrication has been studied.

MoS_2 is considered as a typical representative TMD and has been recently intensively studied. MoS_2 has transition bandgap of 1.2 eV~1.9 eV with the thickness decreased from bulk or few-layer to monolayer. The optical properties of MoS_2 depends on its bandgap structures. With

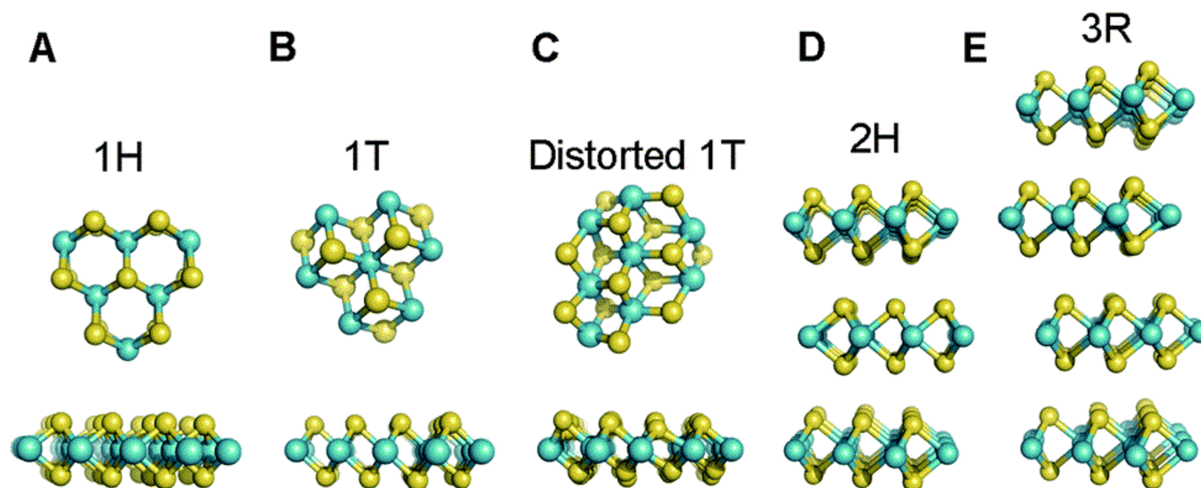

220

221 **Figure 6.** structures of the TMDs.

222 bandgap ranges from 1.2 eV to 1.9 eV, corresponding to wavelengths ranging from 652.6 nm
223 to 1033.3 nm. Linear absorption in the valence band occurs with incident light whose photon
224 energy is higher than 1.2 eV. Photocurrent is generated from the electrons in the conductive
225 band, as shown in Figure 8. Such optoelectronic property and the electrical conductance, as
226 well as carrier mobility of MoS_2 nanosheets show great potential in photodetection with wide
227 band response and high sensitivity.

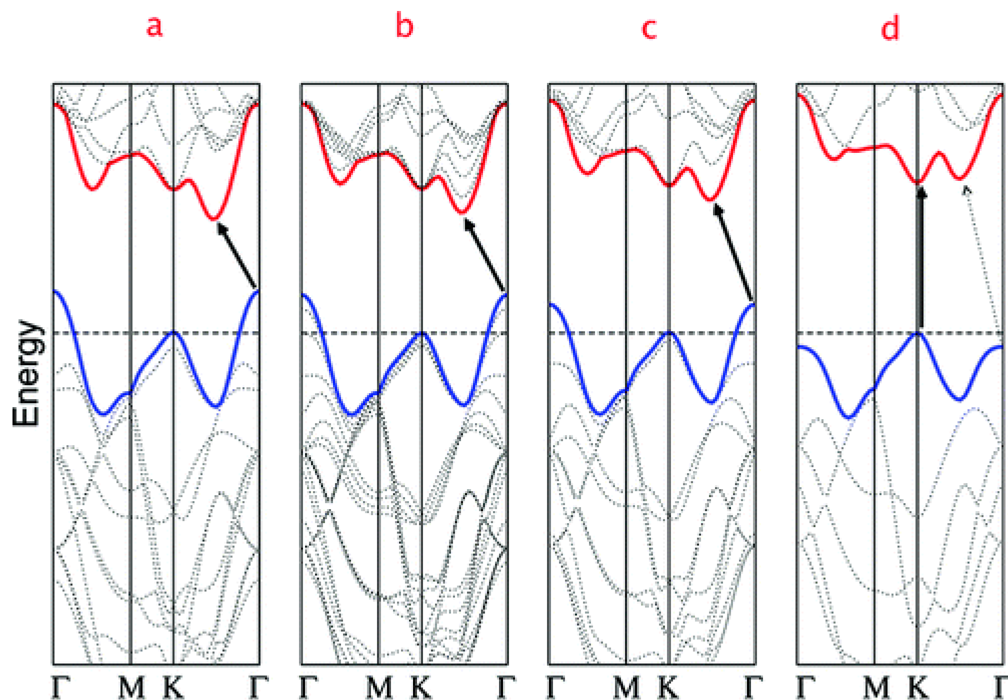

228

229 **Figure 7.** Electrical properties of the layered MoS_2

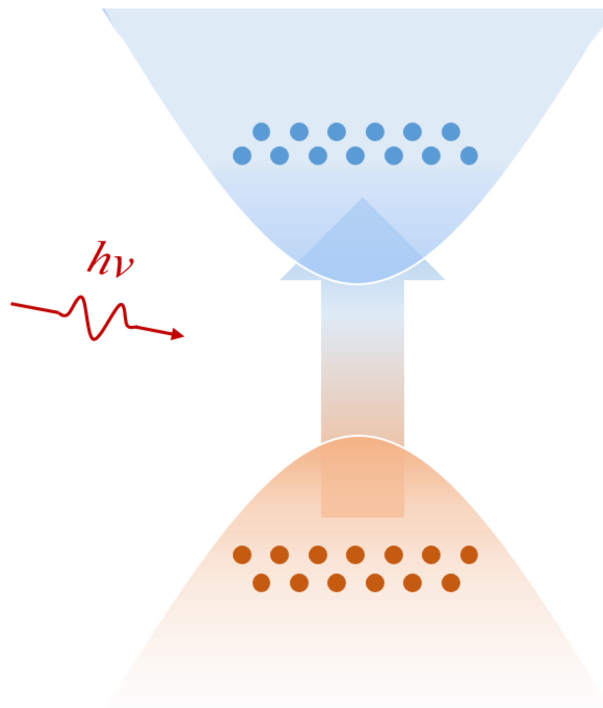

230

231 **Figure 8.** Non-equilibrim carrier generated by incident light

232 2.1.3. Other novel 2D materials

233 Recently 2D materials composed of group-IV (Si, Ge and Sn) elements have also emerged.
234 Silicene and germanene has similar structure as graphene with honeycomb lattice arranged in-
235 plane and Van der Waals bond between adjacent layers. They have application potential in the
236 integrated circuits due to their Si-technology compatibility. Another group IV atomic material
237 that has been intensively studied is stanine whose structure also resembles graphene with two
238 common allotropes: α-tin with face-centered cubic lattice like diamond and β-tin with face-
239 centered tetragonal lattice.

240 Another category of novel 2D materials, the black phosphorus (BP), was first synthesized a
241 century ago and recently attracts lots of interest due to its direct bandgap in bulk and
242 monolayer ranges from 0.33 eV to >1 eV. BP could thus be applied in the mid-infrared
243 photodetectors. Scotch tape method could achieve exfoliated monolayer BP and thickness of
244 monolayer BP could be 0.7-0.85 nm. Structure of the BP is shown in Figure 9. As for the
245 electric properties of BP, the electron and hole mobilityS were measured to be >1000 cm^2V^{-}
246 $^{1}s^{-1}$ at room temperature with high on/off ratio in the application and on/off ratio, together

247 with its band structure, making it suitable for photodetection.[100, 101]

248 **2.2. Fundamentals of ferroelectrics**

249 Ferroelectrics are a group of materials with asymmetry lattice structure, resulting in dipoles in
250 the lattice and capable of being modulated by the external stimuli. One of the most typical
251 characteristics of ferroelectrics is the spontaneous polarization, i.e. the positive and negative
252 charge centers in the original cell of the lattice do not coincide without external electric field

253 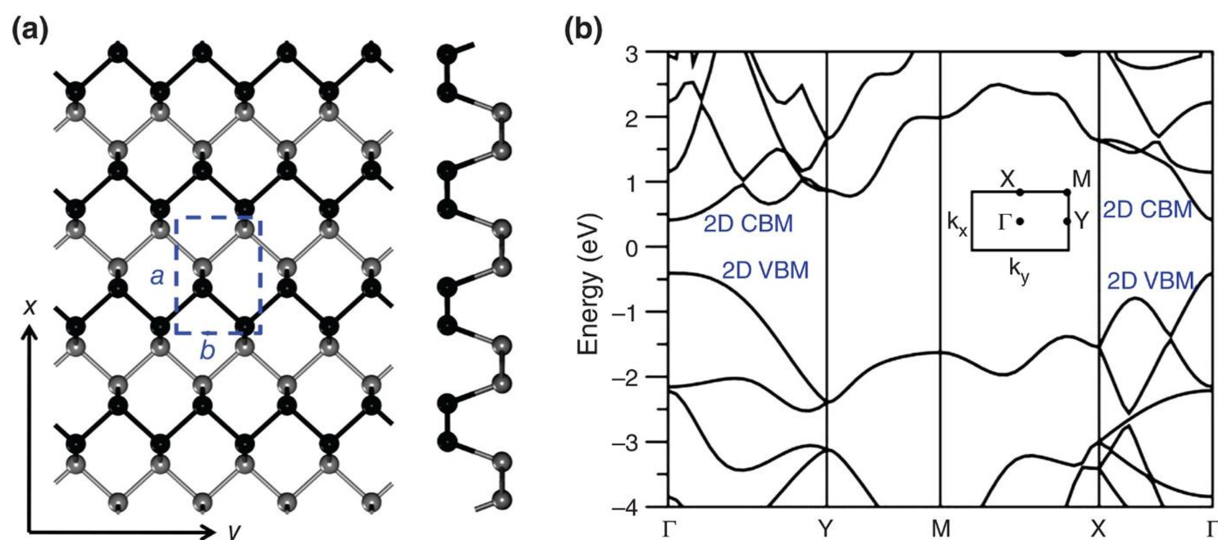

254 **Figure 9.** (a) Lattice structure and (b) electrical band structure of phosphorene.

255 **Table 1.** Bandgap of typical MX_2 (M=Mo, W; X=S, Se, Te)

TMDs	Number of layers	Band gap [eV]	Reference
MoS_2	monolayer	1.9-1.95	[150, 151]
MoS_2	bulk	1.20-1.29	[98, 152, 153]
$MoSe_2$	monolayer	1.44-1.55	[154, 155]
$MoSe_2$	bulk	1.1	[154]
WS_2	monolayer	1.80-2.05	[155, 156, 157]
WS_2	bulk	1.30-1.35	[153, 158]
WSe_2	monolayer	1.65-1.70	[159, 160]
WSe_2	bulk	1.2	[161]
$MoTe_2$	monolayer	0.90-1.10	[162, 163, 164, 165]
$MoTe_2$	bulk	0.88	[164, 165]
WTe_2	monolayer	0.18	[166, 167]
WTe_2	bulk	0.7-0.81	[166, 168]

256 within a certain temperature range. Other properties including the dielectricity,
257 piezoelectricity, pyroelectricity and related effects (for instance electro-optical effect,
258 acoustic-optical effect, photorefractive effect as well as nonlinear optical properties) make
259 them particularly suitable for varieties of applications. These phenomena related to the lattice
260 structure of ferroelectrics could be further investigated by "ferroelectric domain" structure in
261 the materials. Domains are defined as small region of lattice with the same polarization
262 direction, which is correlated to the lattice asymmetry, piezoelectricity and ferroelectricity of
263 the materials. According to the lattice structure, ferroelectrics are categorized into perovskite,
264 pyrochlores, the tungsten-bronze group and the bismuth layer structure group. In combination
265 with 2D materials, the ferroelectrics could be applied as the functional layer due to the alter of
266 polarization with external electric field switching. Typical ferroelectrics including inorganic
267 perovskites with ABO_3 structure, like $Pb(Zr,Ti)O_3$ (PZT), $PbTiO_3$ (PT), $Pb(Mg,Nb)O_3$-$PbTiO_3$
268 (PMN-PT), $BaTiO_3$ (BTO), $(Bi,Na)TiO_3$-$BaTiO_3$ (BNT-BT), $(K, Na)NbO_3$ (KNN) and
269 organic polymers like Poly(vinylidene fluoride) (PVDF) and Methylammonium Lead Iodide
270 ($MAPbI_3$).

271 2.2.1. ABO_3

272 Among all the ferroelectrics, the inorganic ferroelectrics with genetic composition of ABO_3
273 are the most studied and most widely applied. Library of ABO_3 perovskite contains
274 compounds like PZT, PT and BTO, as shown in Figure 10(a).[102, 103, 104] These ABO_3
275 ferroelectrics could be further divided into lead-containing and lead-free compounds. PZT is
276 the dominating ferroelectric materials in the high-end commercial market for its remarkable
277 ferroelectricity and mature ceramic fabrication process. Despite the high performance of
278 devices with lead-containing materials, another group of lead-free oxides like BTO, BNT and
279 BFO are attracting increasing attentions due to their environment-friendly feature and good
280 ferroelectric properties.

281 A-site driven ferroelectric distortions is shown in Figure 10(b).[105] The ferroelectric domain

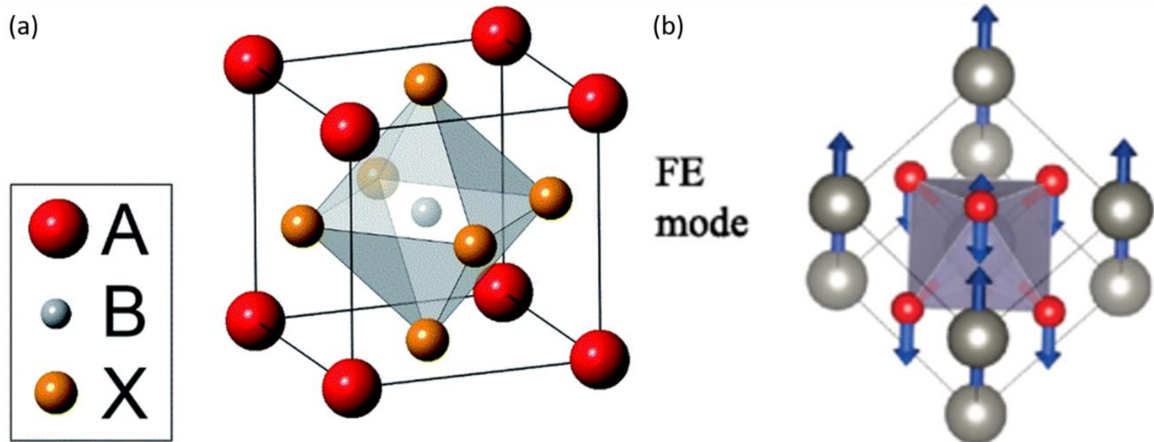

282

283 **Figure 10.** Structure of ABO_3 perovskite

284 strongly impacts the ferroelectricity. Ferroelectric domain refers to a region where the
285 polarization shares the same orientation without any external stimuli. That is to say, all the
286 domain states have the same energy. Furthermore, if an external electric field was applied to
287 the ferroelectric material, polarization tends to be aligned to the same orientation and the free
288 energy would be weakened. Consequently, the permanent polarization could be achieved by
289 applying a large enough external electric field. The most important characteristic of the
290 ferroelectrics is the hysteresis loop, known as the fingerprint of the ferroelectricity, which
291 reveals the non-linear relation between the polarization and external electric field. In addition,
292 the direction of polarization could be reversed by switching the electric field. Different
293 crystallographic forms (e.g. texture, polycrystalline and epitaxial) may significantly influence
294 the material properties and their applications. For instance, the grain and grain boundaries
295 have modulation effects on the polarization and other parameters.[106] Defects in the nano
296 layer structure could lead to stress inside the material and, as well, impact the device
297 performances.[107]

298 Other common methods to characterize the ferroelectricity of materials include the
299 capacitance-voltage (C-V) characteristics, also known as the “butterfly curve”, leakage
300 current and fatigue measurements. Key parameters of ferroelectric materials include the

dielectric constant, coercive field, remnant polarization etc. Figure 11 is the measurements of PZT layer. [108]

Most of the ferroelectrics have intrinsic large bandgap (see Table 2). Ferroelectric thin films possess optical properties including high transparency at visible band, high dielectric constant nonlinear optical response which are particularly useful in lasers for nonlinear optical frequency conversion. In ferroelectric materials, polarization depends on the electric field and incident light, which could be expressed as

$$\vec{P} = \varepsilon_0 \chi^{(1)} \cdot \vec{E} + \varepsilon_0 \chi^{(2)} : \vec{E}\vec{E} + \varepsilon_0 \chi^{(3)} \vdots \vec{E}\vec{E}\vec{E} + \cdots = P^{(1)} + P^{NL}$$

where the first term is the linear optical property of with $\chi^{(1)}$. The $\chi^{(2)}$ and $\chi^{(3)}$, are the

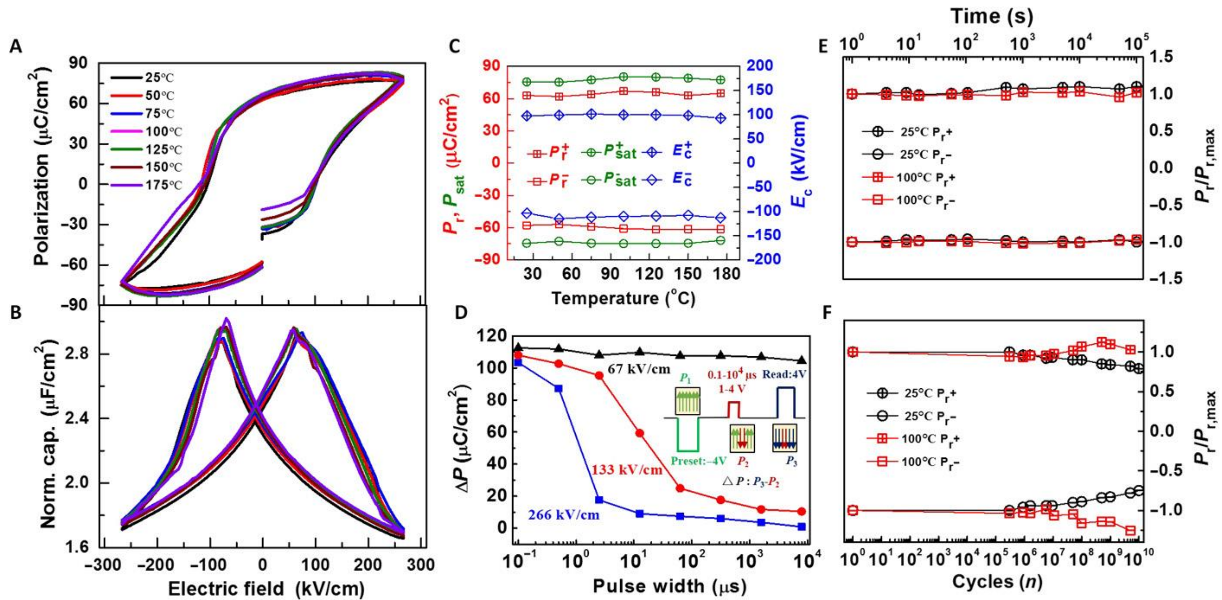

Figure 11. Electrical properties of PZT thin film. (a)*P-E* and (b)*C-E* hysteresis loops at various temperatures. (c) Remnant, saturation polarizations, and coercive field as functions of temperature. (d) PUND switching polarization as a function of pulse width at different voltages. The inset shows the measurement sequence. Retention (e) and fatigue (f) measurements at two typical temperatures second- and third-order nonlinear optical susceptibilities, which correspond to nonlinear optical properties of the material. The second order nonlinearity could induce the sum- and difference-frequency generation, Raman scattering, Brillouin scattering and optical parametric oscillation (OPO) etc. For the third

319 **Table 2.** Bandgap of the typical ferroelectrics

Ferroelectrics	Band gap (eV)	Reference
PZT (Pure)	3.4-4.0	[169, 170, 171]
PZT (Doped)	2.74-3.10	[169]
BTO	2.6	[172]
R' BFO	2.65-2.82	[173, 174]
T' BFO	3.1	[173]
HZO	bulk	[175][175]

320 order nonlinearity of the material, phase conjugation, four-wave mixing and nonlinear
321 absorption could be observed.
322 Polarization of the domains could be modulated by the external optical field. [2, 109] Incident
323 light interacts with ferroelectrics generally in two ways. One is the thermal induced
324 polarization reverse. The incident light with high energy intensity illuminating on the
325 ferroelectrics, which results in continuous increase of temperature in local ferroelectrics and
326 eventually induces polarization switches.[110, 111] It is noticed that such thermal induced
327 polarization switch is irreversible. The other method for light induced polarization switch is
328 based on the open circuit voltage generated from the ferroelectrics, which is also known as
329 bulk photovoltaic (BPV) effect.[112] Li *et al.* has reported the polarization switch by BPV
330 effect in $BiFeO_3$.[113] With light on the surface of ferroelectrics, equilibrium carriers were
331 generated and thus induce photo current I_{ph} in the layer. A build-in electric field was
332 established along the direction of photo current which is, equivalently, considered as a current
333 source. If the build-in electric field could be raise to values higher than the coercive field,
334 polarization of the ferroelectrics can be switched. It is worth mentioning that the polarization
335 is reversible with incident light illuminating on different regions. Moreover, controlling of the
336 strong laser field, tip-enhancement of the light as well as tuning illumination area could also
337 achieve reversible ferroelectric polarization switching, as shown in Figure 12. [114]
338 2.2.2. Ferroelectric Polymers

339 Moreover, organic ferroelectric polymers have also been studied due to their good mechanical
340 property and flexibility. The organic ferroelectric materials are represented by PVDF and its
341 derives. PVDF is one of the most studied material. There are four typical lattice structure in
342 PVDF including α, β, γ and δ phase, which is also known as the I, II, III and IV phases.
343 Structure of PVDF-TrFE was shown in Figure 13. The α-PVDF forms into orthorhombic cell
344 with two chains packing in opposite directions resulting in canceling of the dipole moments,
345 which consequently makes the α-phase PVDF non-polar and paraelectric. β-PVDF shares o-
346 phase as well yet the structure of the lattice is in all-trans planar zigzag conformation with
347 fluorine atoms on one side. β-PVDF could thus achieve the highest dipole moment and

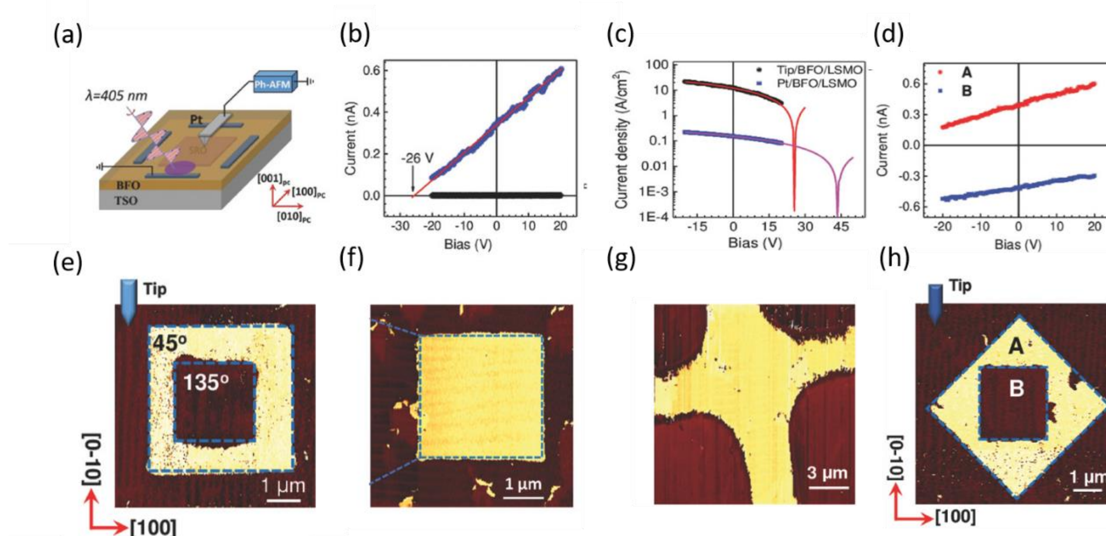

348

349 **Figure 12.** Various methods for the light induced polarization in ferroelectric BFO layer. (a)
350 Schematic illustration of the device and the light incidence. (e) is polarization switching
351 generated from the polarized incident light. (b) is Local current-voltage characteristics with
352 and without illumination at tip-enhancement method and (f) is the corresponding PFM result.
353 (c) is the current density-voltage dependence of tip/BFO/SRO and the Pt/BFO/SRO capacitors
354 and (g) is the PFM amplitude which demonstrated polarization switching with illumination as
355 a result of photocurrent density. (d) and (h) are the polarization switching via tuning
356 illumination.

357

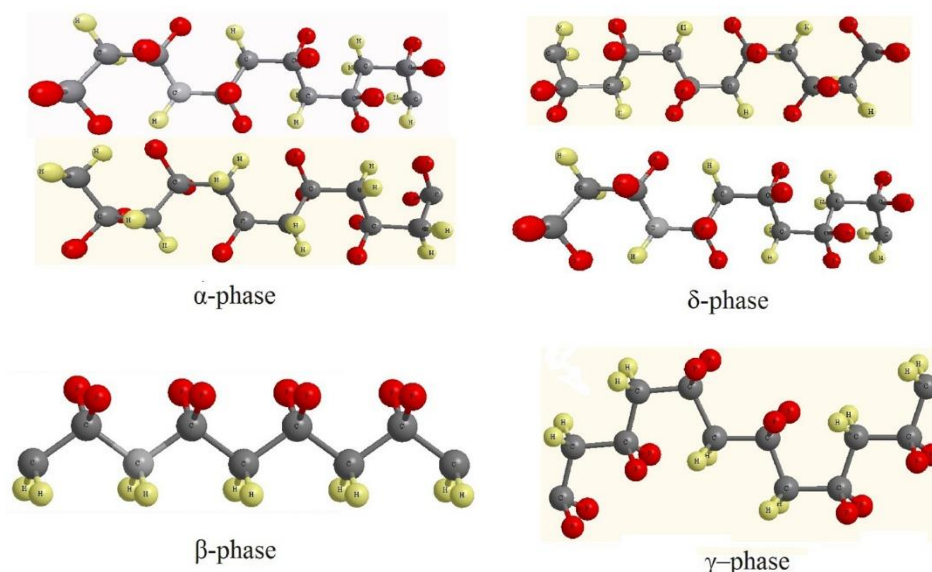

358

359 **Figure 13.** Structure of PVDF crystalline.

360 become the most popular structure of PVDF with the best ferroelectricity and piezoelectricity
361 among all the phases. Crystalline PVDF with γ-phase is monoclinic with partial dipole
362 moment, which also show ferroelectricity. The δ-phase structure resembles the α-phase but
363 with the second chain rotating 180° along the chain axis. Such structure could result in the
364 polar behavior and show ferroelectric property. P(VDF-TrFE) polymer is composed of PVDF
365 and TrFE, which is of the most popular ferroelectric polymers among the PVDF based
366 materials.

367 Incident photons with high energy like X-ray could generate defects in P(VDF-TrFE) and free
368 carriers generated have impact on the reversal of polarization. It was reported that with X-ray
369 illuminating on the polarized P(VDF-TrFE) films, a clear phase difference of 180° as well as
370 domain boundaries was observed. The loss in ferroelectricity will significantly reduce the
371 poled domain area with X-ray irradiation and the domains would be rarely poled after
372 illumination for 60 minutes. [115]

373 **2.3. 2D materials/Ferroelectrics hybrid system**

374 Compared to 2D materials on SiO_2/Si substrates, suspended counterparts MoS_2 has enhanced
375 conductivity. However, if one changes the supporting substrates from SiO_2/Si to other

functional ones, the properties of 2D materials and thus related device performances could be effectively modulated. In addition to holding the 2D materials, these functional substrates play an important part in mechanical, chemical, electronic and optoelectronic properties of the 2D nanosheets. Defects and impurity at the interface as well as the lattice mismatch between the MoS_2 and substrate could all impact the structure of the nanosheets. Then the related charge transfer, interface strain, dielectric screening effect, as well as the optical interference in the 2D semiconductor subsequently impact the device performances.

2.3.1. Electrical interaction of 2D/ferroelectrics hybrid system

Polarization switching in ferroelectrics has been proved to be able to establish a build-in electric field in 2D materials, which could further modulate the electrical properties of the 2D materials.

Therefore, FETs combining 2D materials and ferroelectric layers has been investigated. One of the most typical phenomena observed in the early studies was that the clock-wise hysteresis loop in the transfer property of FET devices, as shown in Figure 14.[116] This hysteresis loop was believed to be originated from adsorbents of water molecules rather than ferroelectric

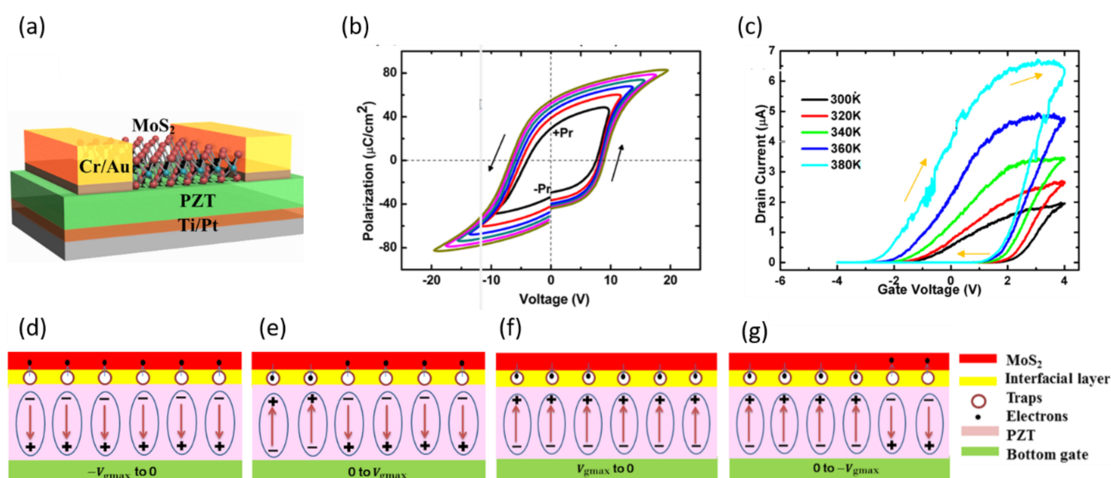

Figure 14. Hysteresis behaviors induced by the interfacial states of MoS_2/PZT FETs. (a) is the devices structure. (b) is the polarization-voltage characterization of PZT film and (c) is the transfer characteristics of the device with anti-hysteresis loop. (d)-(g) is the physical mechanism of charge trapping and de-trapping at the interface of MoS_2/PZT hybrid system.

396 polarization switching which should induce anti-clockwise loop [153,154]. Such clockwise
397 hysteresis was also observed in other 2D materials/ ferroelectrics hybrid system. In addition to
398 water molecules absorbents, other possible reasons like oxide charge trapping and surface
399 charge trapping are also discussed. [117, 118] Hysteresis in ferroelectric devices have
400 undermined the reliability of the devices and scientists have dedicated to solve this issue. Jang
401 et al. has proposed a probable method to eliminate the hysteresis generated from charge
402 trapping in the ferroelectrics. [119] In the devices contain ferroelectric layer, two hysteresis
403 loops with opposite direction exist which is the loop induced by ionic migration in 2D
404 ferroelectrics and loop induced by charge trapping, respectively. These two negative effects
405 might neutralize with each other by modulating the activation energy for ionic migration in

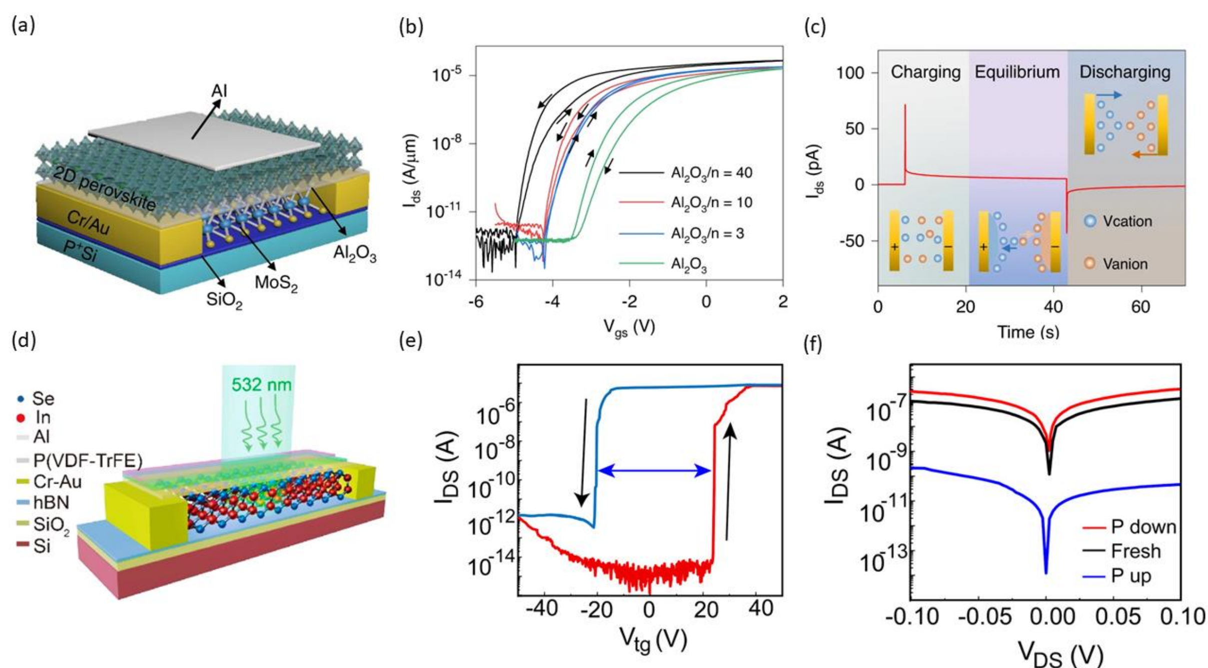

406

407 **Figure 15.** (a) MoS_2 phototransistor with Al_2O_3/2D perovskite heterostructure dielectric. (b)
408 Transfer characteristics of the devices. The neglectable hysteresis loop is achieved. (c) is the
409 schematic illustration of charging-discharging process. (d) is the device structure of InSe
410 photodetectors gated by P(VDF-TrFE). (e) is the anti-clockwise memory window achieved
411 with bias voltage switching from -40 V to 40 V and (f) is the output characteristics of the InSe
412 FET with different polarization states.

413 ferroelectrics, see in Figure 15(a). These rectified devices have proved excellent rectifying
414 characteristics and high performance in photodetection. [120] InSe photodetectors gated by
415 ferroelectrics (shown in Figure 15(b)) has reported anti-clockwise hysteresis in the
416 experiments, as shown in Figure 15(c).
417 Despite the charge trapping induced clockwise hysteresis, the hysteresis generated
418 ferroelectrics could also be observed in the devices as shown in Figure 15 (d). Anti-clockwise
419 memory window was observed with bias applied from -40 V to 40 V, shown in Figure 15 (e)
420 and the electrical properties varied with different polarization states, see Figure 15 (f).
421 In addition to the hysteresis observed in 2D materials and ferroelectrics hybrid system. The
422 dielectric screening effect is capable of modulating the electron-electron interactions as well
423 in the layer adjacent to the substrate, leading to band structures variation and Fermi level shift.
424 Moreover, the electronic transport of 2D materials could be tuned by ferroelectrics with

425 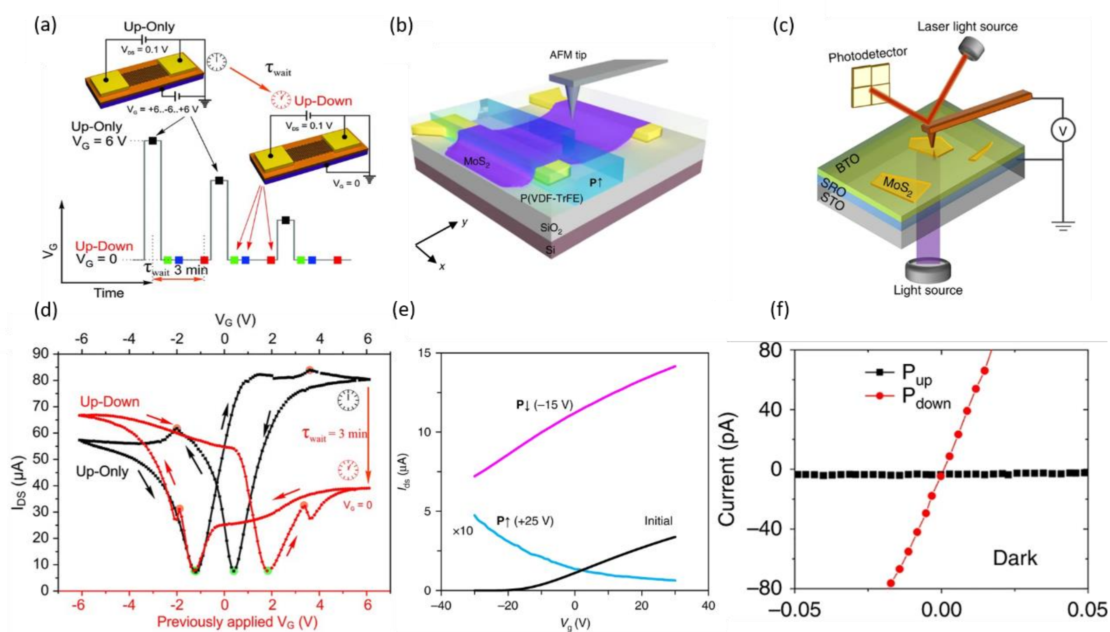

426 **Figure 16.** Electrical properties of the devices modulate by ferroelectric polarization. (a) and
427 (d) are demonstrated the hysteresis reversal in graphene-PZT FeFETs and the I_{ds}-V_{gs} voltage
428 of +25V and down poling voltage of -15V.[122] (c) and (f) demonstrated the polarization
429 induced dark current variation in the MoS_2/BTO FETs.[113]

430 polarized-up and -down were measured.[121] (b) and (e) is the is the I_{ds}-V_{gs} characteristics of
431 MoS2 FETs with PVDF as ferroelectrics and polarized by up poling polarization, as shown in
432 Figure 16.[121, 122, 113] For example, the carrier type of the 2D materials could be
433 modulated by the ferroelectric polarization switching. [123] Reversal of the polarization of the
434 underneath ferroelectric film has led to the conversion of graphene from p-type to n-type,
435 resulting in the reversible switching of the resistance in graphene. Similar results has been
436 achieved by other researches with different 2D materials like MoS_2, $MoTe_2$ and InSe.[122, 45,
437 120] Low-voltage operation could be achieved with high-k ferroelectrics and the retention
438 time of the devices could be improved [159].

439 2.3.2. Optoelectronic properties in 2D/ferroelectrics hybrid system

440 With 2D semiconductor in combination with ferroelectric layers, memory devices are capable
441 of being written and erased both electrically and optically.[14] Moreover, ferroelectric films
442 would be much easier to achieve polarization reversal than the pristine ferroelectrics with the
443 assistance of 2D materials due to the compensation charge generated from 2D materials with
444 incident light. As shown in Figure 17, MoS_2/BTO/SRO structure was fabricated and the

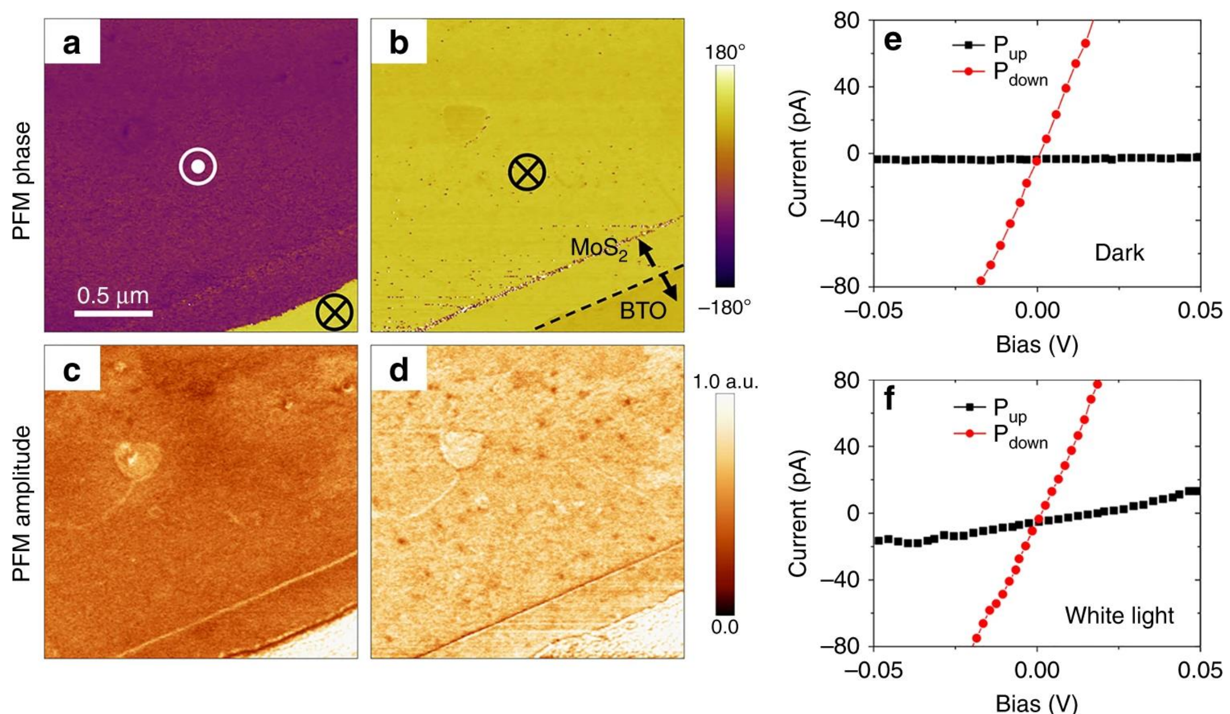

445

446 **Figure 17.** Polarization switching induced by external electric field. [124]

447 underneath BTO was able to be polarized by external electric field with MoS_2 on top. Ultra-
448 violet (UV) light irradiation was then applied in the structure and optical induced polarization
449 reversal was observed, as shown in Figure 17(b)-(e). The illumination of the structure leads to
450 an accumulation of photon-generated carrier at the interface. Charge accumulation could
451 modulate the built electric field and consequently change the electric field applied on the BTO,
452 resulting in polarization switching in the BTO layer.[124] Polarization could also be
453 modulated by the intensity of incident light and the piezo-response microscopy (PFM)
454 amplitude signal, which varied because the photon-induced carriers devoted to the modulation
455 of the electric field at the interface. Similar X-ray induced polarization has been studied with
456 different ferroelectrics. [115]
457 In addition to photon induced polarization reversal with assistance of 2D materials, the impact
458 on optoelectronic properties of 2D materials caused by ferroelectrics has also been observed.

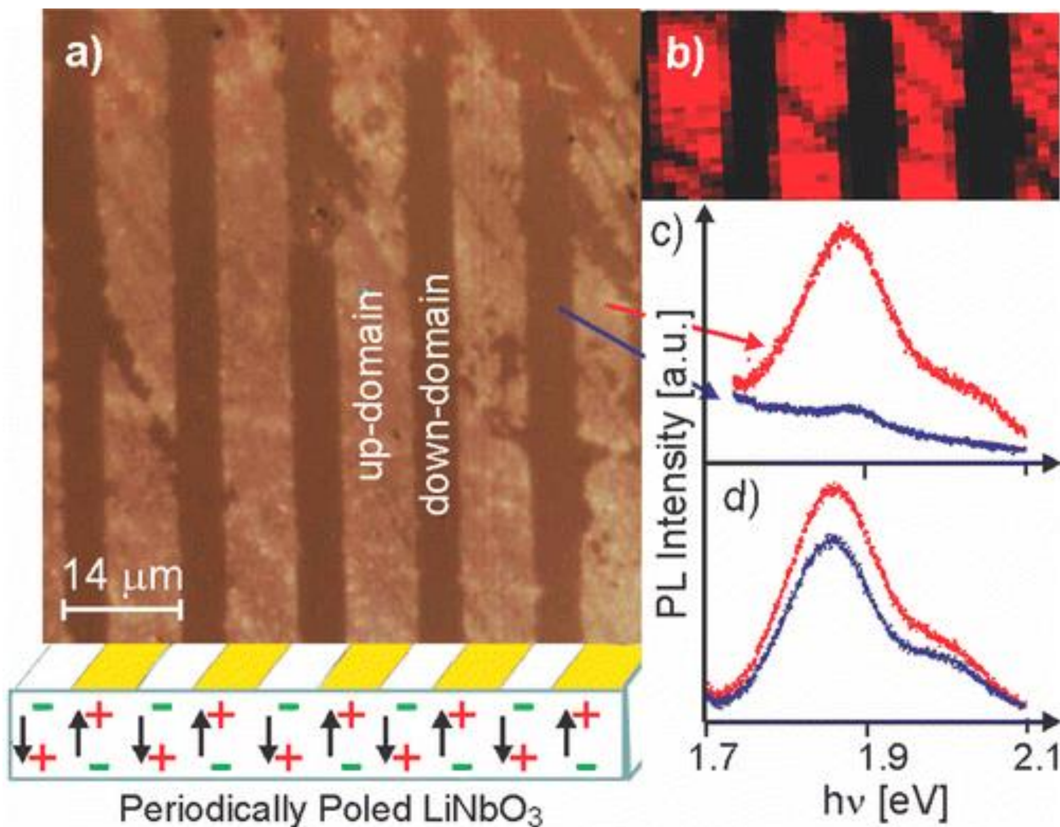

459

460 **Figure 18.** Optical microscopy of selective deposited MoS2 on pre-polarized LN and the
461 photoluminescence of the MoS_2 island. [125]

462 $LiNbO_3$ (LN) is a ferroelectric material widely applied in optical devices thanks to its
463 outstanding nonlinear optical properties. LN could be pre-polarized and applied as substrates
464 for 2D materials. [125] MoS_2 was deposited on the periodically poled LN substrate. Selective
465 growth of the MoS_2 was observed where enhance deposition of MoS_2 was found on the
466 polarization "up" domain compared to polarization "down" domain. Optical properties of the
467 deposited MoS_2 are influenced by the polarized LN, as illustrated in Figure 18. Polarization of
468 the LN substrate could not only influence the growth but also the carrier transport of the MoS_2
469 overlayer.
470 Chemical vapor deposition (CVD) fabrication of MoS_2 requires high temperature of over
471 600°C, which is higher than the Curie temperature of many ferroelectrics and leads to the loss
472 of polarization. Therefore, an alternative method, namely mechanical transfer for the
473 realization of MoS_2 on ferroelectrics has been developed. [126] For instance, CVD grown
474 WS_2 monolayer was mechanically transferred to a pre-polarized ferroelectric substrate and
475 photoluminescence (PL) characterization of the WS_2 was measured. The spatial variation of

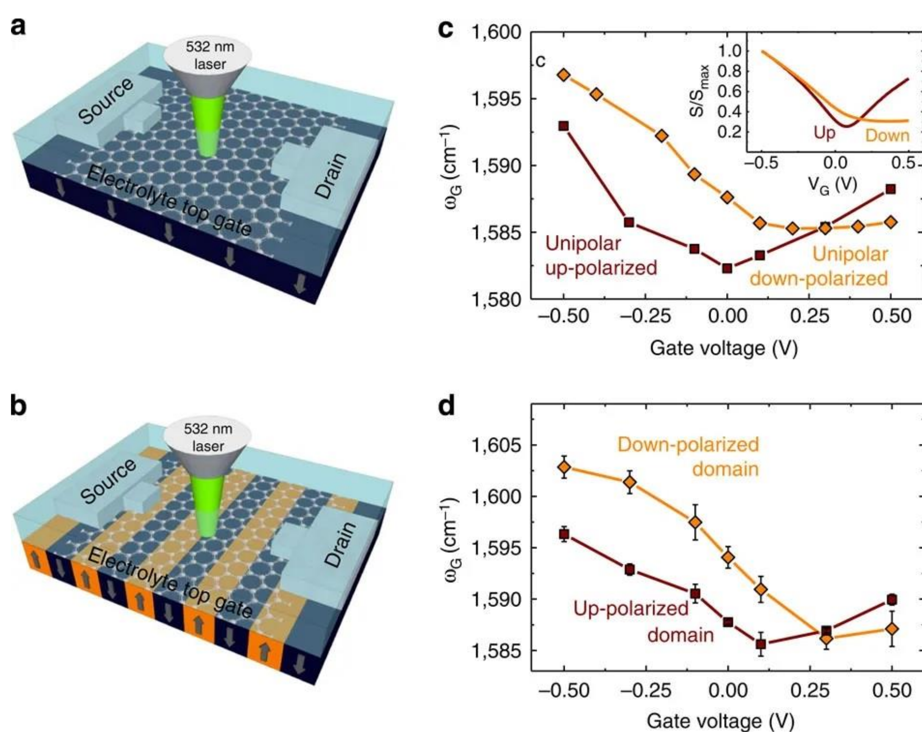

476

477 **Figure 19.** Ferroelectrically driven carrier density modulation in graphene

478

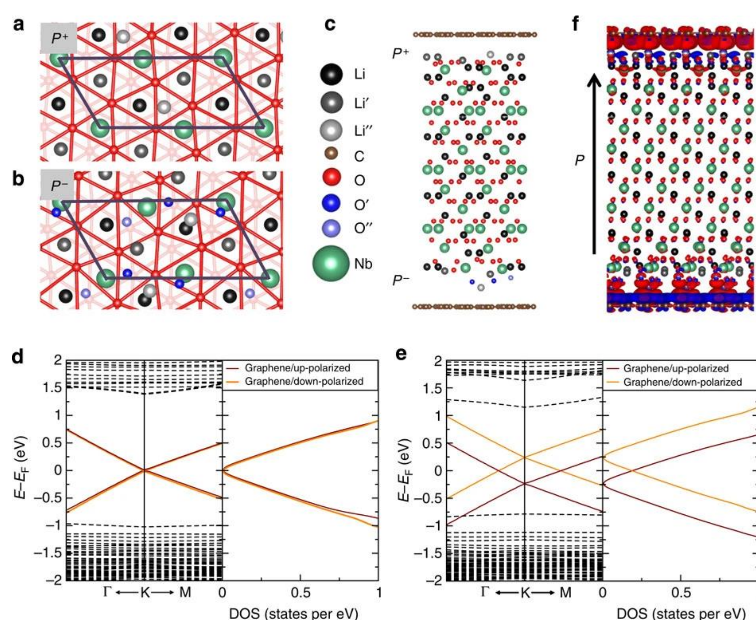

479

480 **Figure 20.** Theoretical study of the ferroelectrically control of carrier density in graphene
481 with first-principle DFT.

482 PL spectra indicates the effective modulation of WS_2 monolayer by ferroelectric polarization.
483 [126]

484 Photo-induced polarization in 2D/ferroelectrics hybrid structure has been proved to be
485 dependent on the intensity of incident light. The ferroelectrics could also drive spatial carrier
486 density modulation in the 2D materials of the hybrid structure,[127] as shown in Figure 19
487 reported by Baeumer *et al.* Characteristic peaks of Raman spectra shift in different
488 polarization domain of the LN crystal. Two orders of magnitude carrier density difference
489 were observed, which could origin from the graphene/LN interfacial chemistry effects. The
490 interaction has also been theoretically calculated by the first-principle density-functional
491 theory (DFT) calculations, as shown in Figure 20. Structure of the interface was constructed
492 and the polarization was applied, as shown Figure 20(f). Calculation of the carrier density in
493 graphene revealed that symmetrical charge densities in graphene was 6.75×10^{12}.

494 **3. Photodetectors based on 2D materials and 2D materials/ferroelectrics hybrid system**

495 **3.1. Fundamentals of photodetection**

496 2D materials with their superior photonic and optoelectronic properties has been extensively
497 studied in nano devices. The TMDs nanosheets are a typical group material among the large
498 amount and types of the 2D materials. The TMDs could be primarily considered as
499 semiconductors with direct or indirect bandgap. Therefore, the principle and understanding of
500 conventional semiconductor photodetection could be transferred to TMDs photodetection.
501 The incident light generates carriers in semiconductors and they are then transported to
502 electrodes. It is noticed that the signal amplification is sometimes applied in this procedure
503 particularly in photodetectors due to the requirement of weak signal detection. Photodetection
504 mechanism mainly consist of the photoconductive effect and photovoltaic effect. There are
505 three main device structures for semiconductor photodetectors, the PN junction and related
506 devices, Schottky junctions and field effect transistors.
507 Semiconductors could absorb the illuminated light and transfer photons to signals like voltage
508 or current. This photodetection process could occur only when the incident photons possess
509 larger energy than the bandgap of semiconductor materials, i.e.

510 $$\hbar v \geq \hbar v_0 = E_g \quad (1)$$

511 where the $\hbar v_0$ is the threshold energy that enables the intrinsic absorption. Moreover, for
512 semiconductors with the indirect bandgap, the probability of the transition is much smaller
513 than that of direct transitions, due to the participation of the phonons. Other absorption
514 including exciton absorption, free carrier absorption and impurity absorption. During the
515 photodetection, electrons in the valence band transit to the conductive band under illumination
516 and generate extra electrons and holes, leading to signals of current or voltage. Photo-
517 generated current could be expressed as

518 $$I_c = q\eta \frac{P}{hv} \quad (2)$$

519 Consider $A = \frac{q\eta}{h\nu}$ is the proportionality constant, which represents the sensitivity of the

520 photodetector.

521 Mechanism of photodetection mainly includes the photoconductive and the photovoltaic ones.

522 The conductivity increases of semiconductors due to light illumination has been briefly

523 introduced before (see section 2.3), which is known as the photoconductive effect, as shown

524 in Figure 21.

525 The generation rate of the photogenerated carriers is proportional to incident light intensity.

526 The photogenerated carriers constantly generate and recombination, the density of photon-

527 generated carriers is

528 $\Delta n_0 = \Delta p_0 = g\tau$ (3)

529 where g is the generation rate of photogenerated carriers, τ is the average carrier life-time.

530 Consider the incident light power of P, g could be written as

531 $g = \eta \frac{P}{h\nu AL}$ (4)

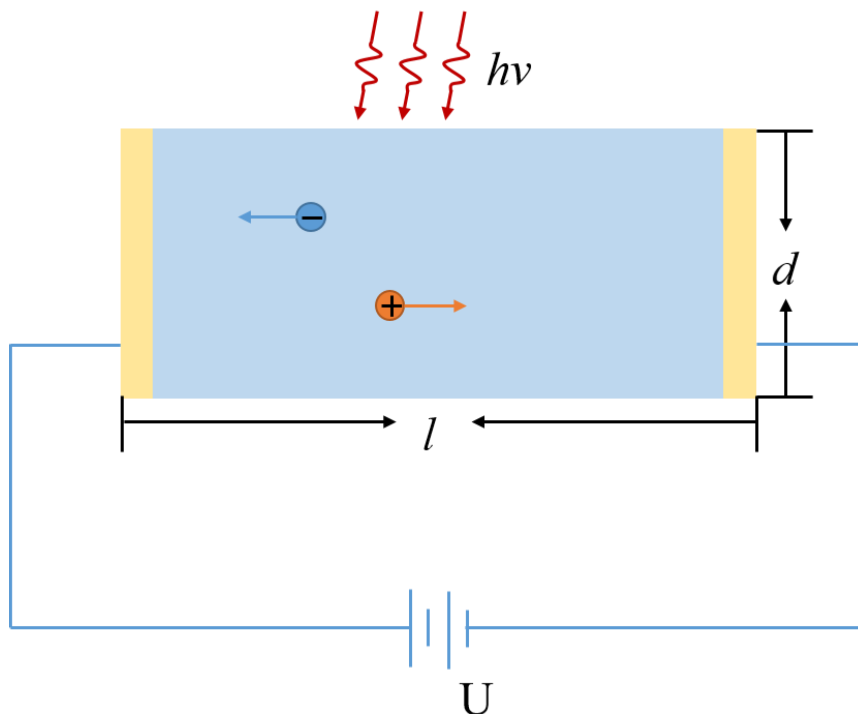

532

533 **Figure 21.** Basic principle of photoconductive current generation

534 where η is the quantum efficiency, A and L is the cross-section area and the length of the
535 material, respectively. Short-circuit photocurrent density with external electric field is

536 $$\Delta J_0 = E \cdot \Delta\sigma = q\tau\eta\left(\mu_n + \mu_p\right)\frac{P}{h\nu AL}E \quad (5)$$

537 Electrical conductivity and photocurrent both increase as the intensity of illumination
538 augments. Photocurrent is then:

539 $$I_p = \frac{U\Delta\sigma A}{L} = \frac{qUA\left(\Delta n\mu_n + \Delta p\mu_p\right)}{L} = \frac{qNU}{L^2}\left(\Delta n\mu_n + \Delta p\mu_p\right) \quad (6)$$

540 where N is the number of generated electron-hole pairs; τ_n and τ_p are corresponding life-
541 time of electrons and holes generated, respectively.

542 With illumination on the inhomogeneous semiconductor, the build-in electric field is formed
543 and photo-generated current is observed when the circuit is shorted. Such optoelectronic
544 effect is photo-voltaic effect.

545 Based on photoconductive and photovoltaic mechanism, different devices are developed, in
546 which photoconductors and photodiodes are two typical representatives. Photoconductors are
547 based on photoconductivity. Photo-conductors usually has wide band response, relatively high
548 operating current and high sensitivity. With the incident light, the non-equilibrium carriers
549 increase and consequently improve the conductivity of the materials, and the resistance is thus
550 reduced under illumination.[128, 129] The photoconductive effect is sensitive to the
551 nanostructure as well as the doping and defects of the semiconductors. Photoresistors based
552 on 2D materials with wide band responsivity has been widely studied and reported by
553 researchers. [130] It was demonstrated that the 2D materials are able to cover the UV to infra-
554 red band with high responsivity and ultrasensitive properties.

555 Photodiodes are based on the photo-voltaic effect, which is also known as barrier-type
556 photodetectors. Photodiodes include PN junction, the PIN junction, heterostructure and
557 Schottky diodes.

558 Compared to photoconductors which require external voltage, photodiodes have certain
559 polarities and thus the signals could be transferred without external voltage. Photodiodes also
560 show fast responsivity and good frequency response.
561 Taking PN junction as an example to explain the photodetection process, the barrier region in
562 a PN junction shares relatively strong build in electric field (from n-region point to p-region).
563 Photo-generated carriers move in opposite directions under the build-in electric field. The
564 electrons in p-region move to the n-region while the holes enter the p-region. Such movement
565 of the electrons and holes consequently lead to potential reduction in the n-region and rise in
566 the p-region. Electromotive force (EMF) across the PN junction generated with illumination
567 results into a pressure drop $qV_D - qV$ and forward current I_F .In addition to the photoresistor
568 and PN diode, another group of devices enable photodetection could are as well studied
569 profoundly, known as the phototransistors.

570 **3.2. Figures of merit in photodetection**

571 The most important parameters for photodetection are identified as speed, responsivity and
572 sensitivity. Other parameters including quantum efficiency, noise and gain are important
573 figures of merit as well. It is noted that here we only consider the semiconductor
574 photodetector to understand the operation of the semiconductor photodetector and figures of
575 merit for photodetection which are of vital importance to the materials parameters, device
576 structure and performance. Definitions of the parameters of quantum efficiency, responsivity,
577 sensitivity, response speed and photo gain are as follows:

578 "Quantum efficiency" could be divided into internal and external quantum efficiency, which
579 are the most important parameters for semiconductor optoelectronic photodetectors. The
580 internal quantum efficiency (IQE) is define as the number of electron-hole pairs generated by
581 absorbing one incident photon, which is

582 $$IQE = 1 - e^{-\alpha(\lambda)W} \quad (7)$$

583 where $\alpha(\lambda)$ is the absorption coefficient of corresponding wavelength λ, W is the thickness
584 of the absorption layer. It is demonstrated that the IQE increases with the absorption
585 coefficient or the thickness of the absorption layer grows. In practical applications, there is no
586 way for photons reach the absorption layer through the surface of the materials. Photons go
587 through a heavily doped contact area with photon loss rather than passing through the surface
588 of materials to reach the absorption layer. Simultaneously, the reflection of the surface also
589 consumes part of the incident photons. Thus, the external quantum efficiency (EQE) is
590 defined as

591
$$\begin{aligned} EQE &= \left(1-R_f\right)e^{-\alpha(\lambda)d}\cdot IQE \\ &= \frac{I_p/q}{P/hv} \end{aligned} \qquad (8)$$

592 where d is the thickness of contact area and R_f is the surface reflectivity on photodetector.

593 "Responsivity" of a photodetector is the voltage or current of photodetector output divided by
594 the input power, which could be categorized into spectral responsivity (R_λ) and integral
595 responsivity (R). If the photo-induced current (I_{ph}) is measured with incident power of P,

596
$$R = \frac{I_{ph}}{P} \quad (9)$$

597 according to the definition of quantum efficiency, then

598
$$R = EQE\cdot\frac{q}{hv} \quad (10)$$

599 where q is the electronic charge.

600 "Sensitivity" of a photodetector is the minimum photon signal detected under certain
601 transmission bandwidth and rate. It measures the photoelectric conversion characteristics, as
602 well as the spectral and frequency conversion characteristics.

603 "Response speed" of photodiode is evaluated by the rise/fall time (τ_r/τ_f) of the detective
604 signal. The response speed is defined as the frequency where the photocurrent decreases to
605 $1/\sqrt{2}$ from peak in frequency domain. Incident photons will go into the semiconductor
606 through the surface layer, then photo-generated carriers and free electron-hole pairs shift
607 under the electric field. The time required for incident photons to be transferred to
608 photocurrent is the "response time". Three main factors could affect the response time,
609 including the diffusion and transition time in the depletion region, as well as the RC time
610 constant of the photodiode.
611 The "noise equivalent power (NEP)" is another key parameter for photodetection, which
612 refers to the input signal power which results in a signal-to-noise ratio (S/R) of 1 in a 1 Hz
613 output bandwidth. [131]NEP has expressed the sensitivity of photodetectors. Another typical
614 parameter being correlated to the NEP is the "detectivity" (D^*).

615 $$D^* = \frac{(A \cdot \Delta f)^{\frac{1}{2}}}{NEP} \quad (11)$$

616 where, A is the area of the photosensitive region and the Δf is the frequency bandwidth of the
617 detector.
618 "Photogain" is a benchmarked parameter for photoconductive detectors, which is

619 $$G_{ph} = (I_{ph}/q)/(\Phi_{in}QE) \quad (12)$$

620 where $\Phi_{in} = \frac{P}{hv}$ is the incoming photon flux. Here we bring another definition of External
621 Quantum Efficiency (EQE) for sensitized photoconductors as $QE = \eta_{trans}\eta_{abs}$, where η_{trans} is
622 the charge transfer efficiency and η_{abs} is the absorption efficiency, which demonstrates the
623 number of detected charge carriers per single incident photon. The photogain can also been
624 quantified by the ratio of the lifetime of the trapped carriers (τ_{life}) over the drift transit time
625 ($\tau_{transit}$). If we take a FET for example, a bias (V_{bias}) is applied to a FET device, the G_{ph} can

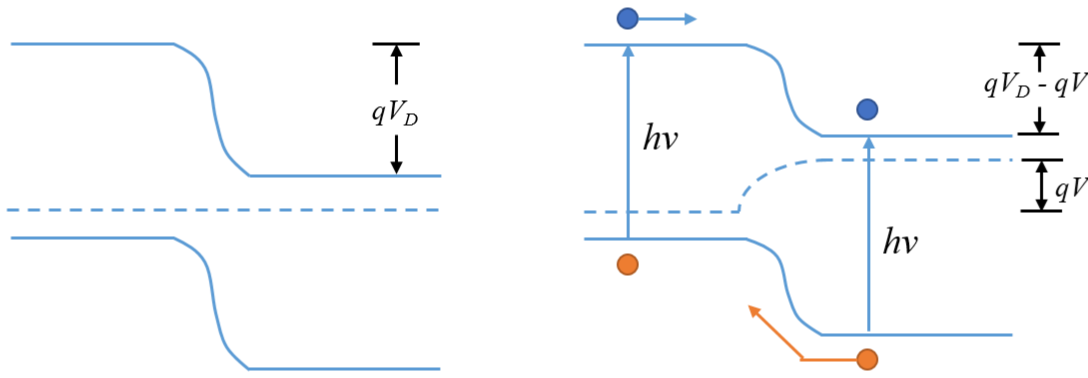

626

627 **Figure 22.** Band structure of PN junction and the mechanism of photodetection.

628 be defined as

629 $$G_{ph} = \frac{\tau_{life} \cdot \mu \cdot V_{bias}}{L^2} \quad (13)$$

630 where L is the channel length, μ is the carrier mobility.

631 **3.3. Photodetectors based on PN junctions**

632 For 2D materials, iron-doping and adsorbates of the materials are often applied to achieve p-
633 type or n-type semiconductors, as shown in Figure 22. Structure of 2D materials applied in the
634 devices are basically categorized into the homojunction and heterojunction. Detectors based
635 on various 2D materials has been reported. [132] Graphene PN junction was formed by
636 applying voltages with opposite polarities on the top and bottom gate, as shown in Figure
637 23(a)-(c). Thermo-induced carriers were considered to play an important role in the
638 optoelectronic response of graphene, and the photocurrent was demonstrated to be >40 nA
639 with a relatively low voltage bias and an incident light with the wavelength of 850 nm.
640 Responsivity was correspondingly measured to be 5 mA W^{-1} which was relatively small
641 compared with FETs photodetectors, yet larger than the previously reported 1 mA W^{-1}. MoS2
642 homojunction photodetectors with a ultra-high responsivity of 7×10^4 A W^{-1} and EQE>10%
643 has been reported by Huo *et al*. [133] p-type and n-type MoS_2 was achieved by chemical
644 doping and form a vertical junction as

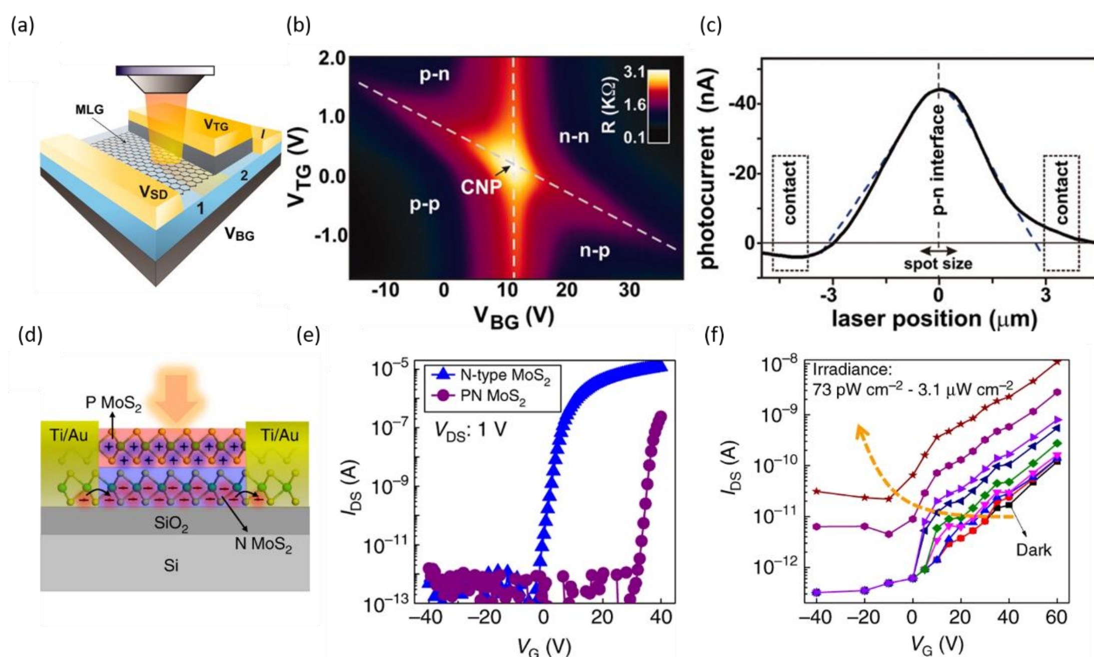

645

646 **Figure 23.** (a)-(c)Photodetectors based on graphene homo-junction and the photocurrent with
647 incident light. (d)MoS2 homojunction photodetector, (e)electrical properties of the devices
648 and (f) photocurrent generated with light illumination.

649 shown in Figure 24(d)-(f). Moreover, TMDs including WSe_2, WS_2, $MoTe_2$ et al. have been
650 utilized in the photodetectors. [134] The photodetectors using 2D materials heterojunctions
651 have also been investigated and optimized in many aspects, which are summarized in Ref.
652 [135, 134, 136].

653 Lv et al. has also reported on the 2D photodetectors with MoS_2 homojunction. [122] Doping
654 in MoS_2 channel was reconfigurable by ferroelectric polarization. Polarization upward of
655 P(VDF-TrFE) with was applied as ferroelectric layer in the experiments due to its remarkable
656 coercive field of ~5×10^7 V m^{-1}. The MoS_2 channel turned into p-type semiconductor with
657 upward polarization and reversal of external electric field resulted in switch of majority
658 carriers, as n-type doping were enhanced in the MoS_2 channel. 10^9-10^{13} cm^{-2} doping in MoS_2
659 was achieved by ferroelectric polarization. It is noticed that voltage applied in polarization
660 process varies with different channel materials (eg. $|V_p|<10V$ with MoS_2 and $|Vp|=\pm6$ V with
661 WSe_2).As shown in Figure 24, responsivity of the photodetector has reached up to 10^2.

662

663 **Figure 24.** Performance of the MoS_2 homojunction photodetectors.

664 PN junctions based 2D-ferroelectrics hybrid structures are also studied, in which the
665 polarization of ferroelectrics could induce carrier transport of 2D materials. Responsivity of
666 the device was kept in the magnitude with UV spectrum, which confirmed the function of the
667 photodetector at UV region. Moreover, ferroelectrics applied in the photodetector could
668 effectively influence the device performance. [137]

669 In addition to the devices based on MoS_2 with ferroelectrics, similar researches have been
670 carried out with various materials. Wu et al has reported $MoTe_2$ PN junction defined by
671 ferroelectrics, as shown in Figure 25.[45] PN junction could be converted to n-p, n-n and p-p
672 doping by external voltage pulses, as shown in Figure 25(b). Such modified photodetector
673 under illumination of different wavelengths including 520 nm and infrared was investigated
674 (see Figure 25(c) and Ref [45]). Other figures of merit including EQE and responsivity were
675 studied as well and on/off ratio of 5×10^5 was achieved. The responsivity could reach 5 A W^{-1},
676 detectivity was 3×10^{12} Jones as well as fast response time of 30 μs. Such PN junctions enable
677 photodetection unveiled opportunities for advanced nano photodetectors and realizing next-
678 generation optoelectronic devices.

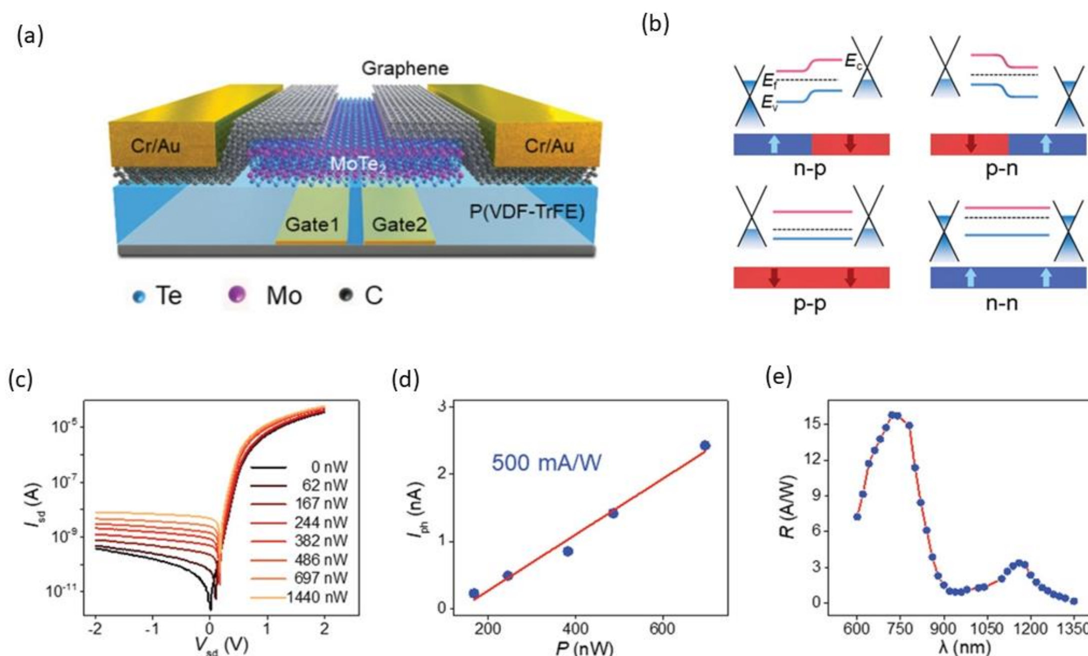

679

680 **Figure 25.** (a) MoTe2 PN junction controlled by ferroelectric domains. (b) switchable doping
681 method defined by polarization. (c)-(e) are devices performances under different illumination.

682 **3.4. Photodetectors based on field effect transistors**

683 Photodetectors based on 2D materials FETs with monolayer graphene as the channel were
684 reported in 2008 for the first time. [138] Zero-bandgap graphene has the advantages of wide
685 band response, which allows facile generation of photocurrent by the incident light.
686 Photocurrent of the graphene photodetector with 514.5 nm incident light reached a maximum
687 of ~350 nA with the gate bias varied in a relatively large range (-40 V-40 V), and the
688 photocurrent modulation by the gate bias was obviously observed in the devices, as shown in
689 Figure 26(a)-(c). Suspended graphene monolayer has high Fermi velocity (~1/300 of the
690 speed of light in vacuum) and huge electrical mobility (200,000 $cm^2V^{-1}s^{-1}$). Photocurrent of
691 the graphene FETs photodetectors has reached over 1 μA and the maximal responsivity was
692 0.5 mA W^{-1}. [28] For optical communication, the photoresponse in communication band is a
693 priority. Graphene has responsivity of 6.1 mA W^{-1} at the wavelength of 1550 nm. Back gate
694 monolayer graphene photodetectors at a data rate of 10 Gbit s^{-1} at 1550 nm incident light was
695 achieved, as shown in Figure 26(d)-(f).

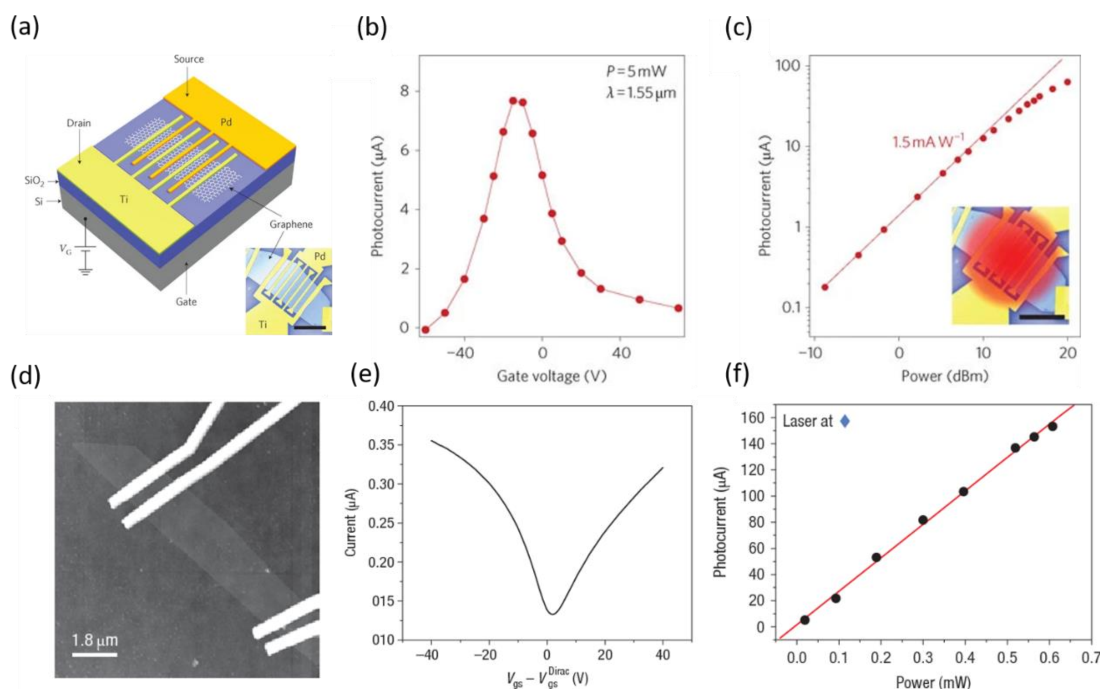

696

697 **Figure 26.** (a)-(c) is Graphene photodetectors where (a) is the structure of the devices, (b) and
698 (c) are the photocurrent dependent on the gate voltage and incident power intensity,
699 respectively.[138] (d)-(f) is Back gate monolayer graphene phototransistors enable high speed
700 photo communication.[28]

701 Besides graphene other 2D materials, for instance the CNTs, TMDs and h-BN etc. have been
702 also applied in photodetection inspired by graphene FETs photodetectors. Similar MoS_2
703 monolayer FET structures and devices have been reported, firstly by Yin et al. in 2011[129]
704 One of the most prominent properties of the MoS_2 different from graphene is that monolayer
705 MoS_2 has an intrinsic bandgap of 1.8 eV, which enables MoS_2 to be “switched off” in the
706 FETs. However, the pristine MoS_2 has relatively low mobility ranging from 0.5 $cm^2V^{-1}s^{-1}$ to 3
707 $cm^2V^{-1}s^{-1}$, [139] which could result in the impurity scattering and remote charge. High-*k*
708 dielectrics could be good in improving the transport properties which could provide charge
709 screening and reduce the trap/impurity scattering, then could consequently improve the carrier
710 mobility. Inorganic HfO_2 and Al_2O_3 are among the most studied dielectrics, for the organic
711 materials, PVDF is a typical material that was utilized as the gate insulator. The mobility of
712 MoS_2 could be increased by two orders of magnitude, together with high on/off ratio of 10^8

713 and is thus very promising in the device applications [140]. In MoS_2 FET photodetectors,
714 photocurrent is linearly proportional to the power of incident light High on/off ratio with ~10^8
715 could be achieved by high-k dielectrics like PZT, HfO_2 and Al_2O_3. On/off ratio for the simple
716 back gate monolayer MoS_2 with SiO_2 as gate insulator was measured to be 10^2-10^3, and the
717 delay was at ~50 ms. [129] The back gate monolayer MoS_2 FET was fabricated and the
718 photoresponsivity was 7.5 mA/W with low power incident light (P=80 μW) and medium gate
719 bias (V_g=50 V) [129].
720 FET Photodetectors based on TMDs, BP and h-BN with remarkable photoresponse has also
721 been studied and shown. Improvement of the devices performance and novel phenomena were
722 found and discussed. 2D material heterostructures was achieved to realize the photodetection
723 [141]. More recently, many studies are devoting themselves to realize flexible and transparent
724 photodetectors using 2D materials, which are of great interest for the future applications of
725 wearable and solar-energy devices.
726 Photodetectors based on 2D materials modulated by ferroelectrics has been reported since
727 2015. Initially ferroelectrics were introduced to 2D FET photodetectors only thanks to their
728 high-k property, which can be used to enhance the photodetection performance. Wang *et al.*
729 are among the first groups demonstrating MoS_2 based 2D photodetectors driven by
730 ferroelectric P(PVDF-TrFE) and they proposed the device structure as shown in in Figure
731 27.[142] Few layer MoS_2 was used as semiconducting channel while the P(VDF-TrFE) was
732 employed as the gate insulator. Dark current with non-polarized P(VDF-TrFE) was measured
733 at 10^{-7}-10^{-8} A and could be depressed to <10^{-10} A with polarized-up P(VDF-TrFE). Signal-to-
734 noise-ratio reached 10^3 using polarized gate. Illuminated by an incident light with a
735 wavelength of 635 nm, the photocurrent of the device reached >50 μA at a low power of 1nW
736 and 5 V source-drain voltage. Meanwhile, the stable polarization of P(VDF-TrFE) provided a
737 high electric field (~10^9 V m^{-1} within the nanometer scale) thus keeping the MoS_2 channel in
738 the fully depleted state, which significantly improved the sensitivity of the detector. The

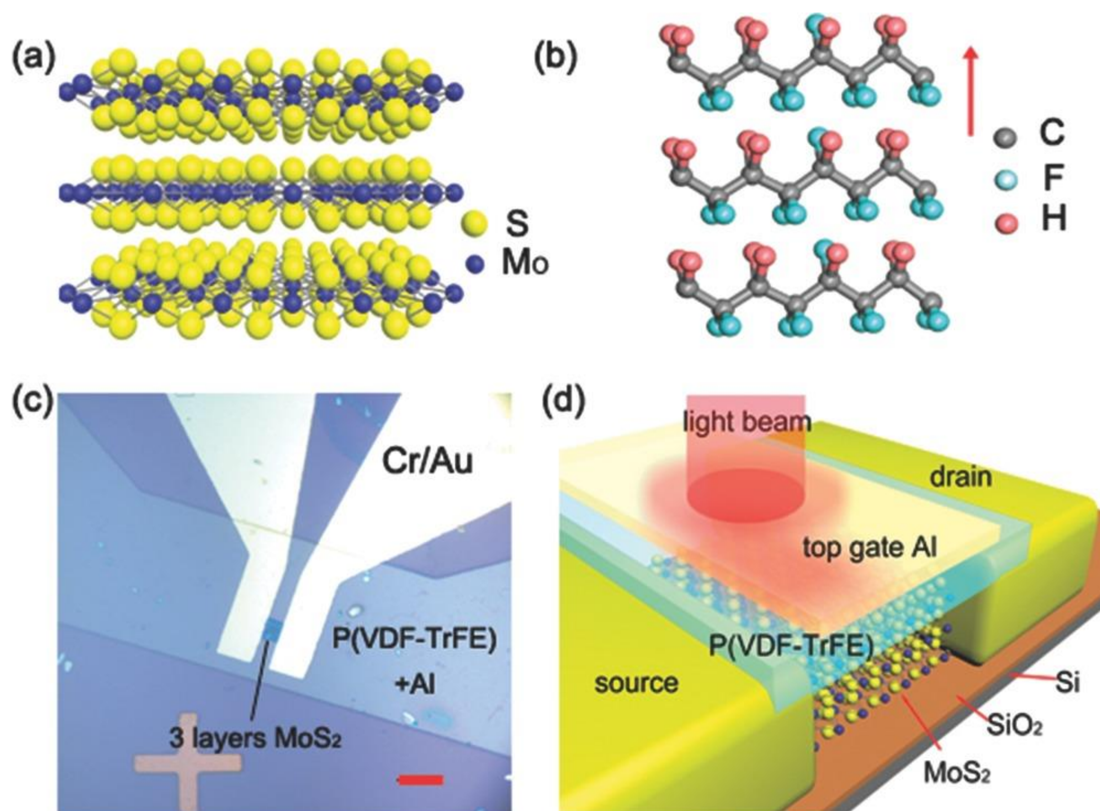

739

740 **Figure 27.** Ultra-sensitive MoS_2 photodetectors with ferroelectrics

741 photodetector reached quite a high detectivity ~2.2×10^{12} Jones and a responsivity up to 2570

742 A W^{-1}.

743 Similar 2D-ferroelectrics phototransistors have recently been extensively studied and

744 reported. Wide band photodetection (from visible light to 1550 nm) was achieved and the

745 relative high sensitivity >340 A W^{-1} was measured with an incident light wavelength of

746 450nm.[143] Considering that both the crystalline structure of ferroelectric gate materials and

747 the carrier transport fluctuation in the 2D materials strongly depend on the temperature

748 variation, the temperature dependence of the 2D-ferroelectrics hybrid FET photodetectors

749 have been studied. Chen *et al.* has reported that a low temperature of 200 K could transform

750 the lattice structure of P(VDF-TrFE-CFE) into ferroelectrics/relaxor, which changes the

751 property of P(VDF-TrFE) and could further modulate the band structure of the few-layer

752 MoS_2 material, enabling the long wavelength detection to 1550 nm, as shown in Figure

753 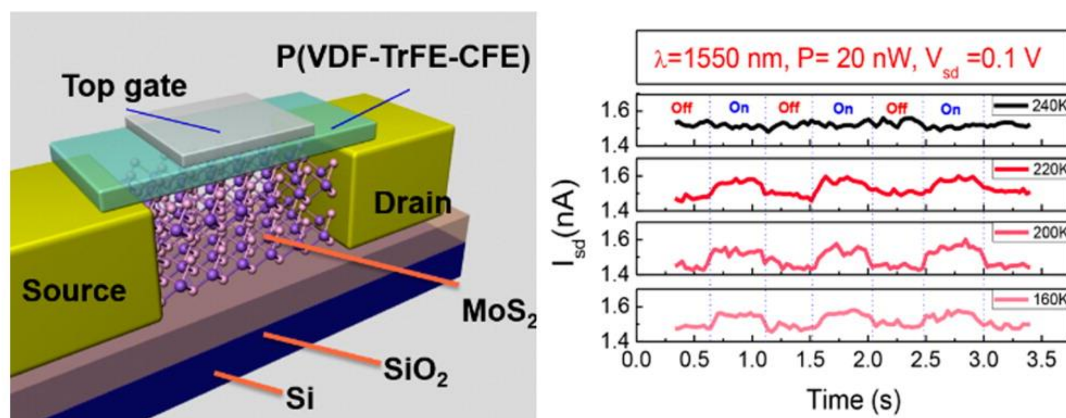

754 **Figure 28.** Schematic illustration of the MoS_2 photodetectors driven by ferroelectric gate and

755 the temperature dependence of the response at 1550 nm incident light.

756 28.[143] Screening coulomb impurities of ferroelectrics could also enhance the carrier

757 mobility of MoS_2.

758 On-off ratio and delay are another two key figures of merits of the 2D-ferroelectrics hybrid

759 photodetectors. On/off ratio of the devices was determined at zero gate bias at a low drain

760 currents, while delay time of the devices accounts for the time required to switch the device

761 on. Both on/off ratio and delay time express the response speed of the devices. On/off ratio

762 for the monolayer MoS_2 based nano electronic devices could reach up to 10^8 [144]and the

763 simplest back gate FETs as photodetectors have an on/off ratio of 10^2-10^3[145]. Application

764 of the ferroelectrics has been proved to be able to significantly improve the sensitivity, the

765 on/off ratio and the SNR of photodetector. On/off ratio of MoS_2 photodetector with P(VDF-

766 TrFE) applied as ferroelectric gate was increased to $>10^4$ with dark current approximately to

767 10^{-11} A [146].

768 In the 2D-ferroelectrics hybrid photodetectors, some unique properties of 2D materials, like

769 the plasmonic behaviors of graphene, could be modulated by the ferroelectrics, which further

770 improve the photodetection performances. An ultra-high responsivity up to 7.62×10^6 A W^{-1}

771 has been reported graphene-ferroelectrics photodetectors, which is much beyond the

772 previously reported experimental results. Meanwhile, detectivity reached ~6.24×10^{7} Jones
773 with infra-red band photodetection. [147] Graphene was transferred on the pre-polarized
774 ferroelectric substrate and the graphene plasmons was excited by the polarized domains.
775 Graphene plasmons resonates at the boundaries, as shown in Figure 29. Polarized domains at
776 the substrate could modulate the carrier density and the chemical potential (namely the Fermi
777 level) of graphene by the external electric field. Broad band photodetector with wavelengths
778 ranging from 5μm to20μm was achieved, as shown in Figure 30.
779 For the extensive investigation of 2D materials and ferroelectrics. There is a group of unique
780 2D semiconductors, represented by α-In_2Se_3, shares both semiconductor property and the
781 ferroelectricity. The combined properties make it potential in the ultra-thin photodetectors due
782 to its capability of playing a dual role in the application of photodetectors. Hou et al has
783 reported the α-In_2Se_3 applied in the photodetectors, as shown in Figure 31. [148] Polarization
784 of α-In_2Se_3 pull the electrons to the surface of the materials and consequently forms into an
785 electric field, which would influence the electrical properties of the photodetectors. On/off
786 ratio of the photodetector was measured to be 2×10^{7} and the comparison of the photodetector
787 with and without polarization demonstrated that the polarization could prolong the decay yet
788 significantly improve the on/off ratio with even three orders of magnitude, and

789 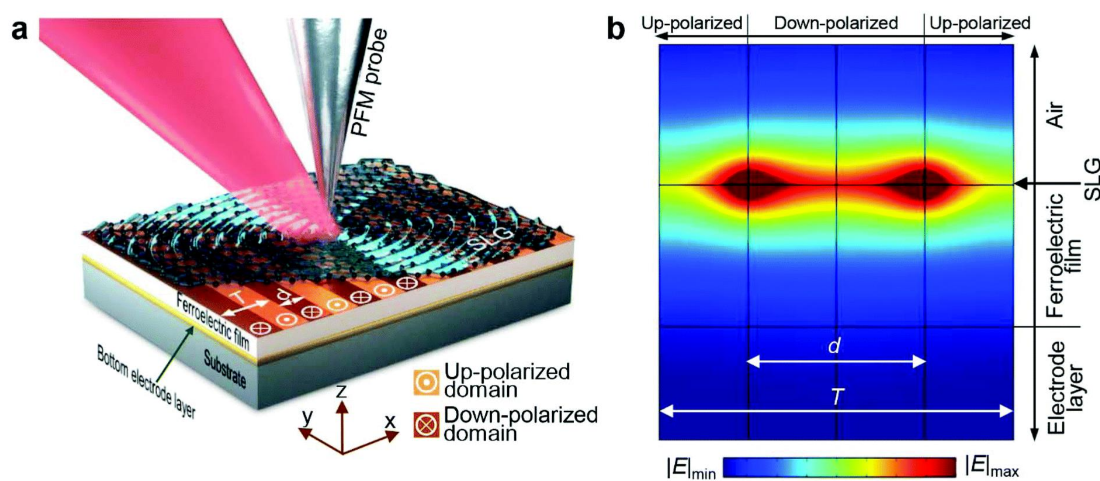

790 **Figure 29.** pre-polarized graphene photodetector and the plasmons excited by the polarized-
791 up and -down domains

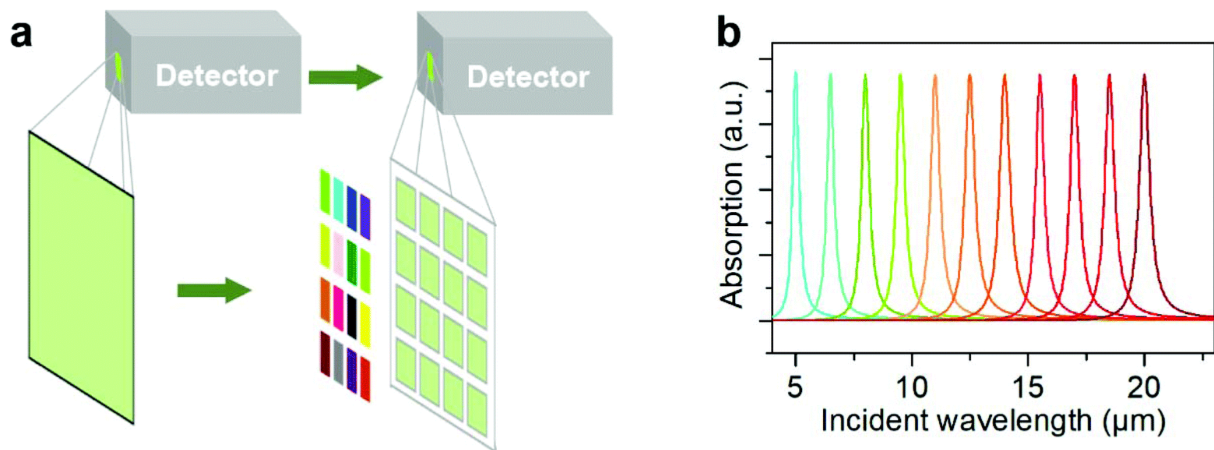

792

793 **Figure 30.** Graphene plasmonic photodetector controlled by ferroelectric domains and the

794 wide-band response

795 Photodetectors with Pt electrodes could further optimize the on/off ratio by four orders of

796 magnitude.

797 In addition to traditional ferroelectrics, recent emerged ferroelectric semiconductors have also

798 attracted many interests and have been applied into 2D-ferroelectris hybrid photodetectors.

799 The ferroelectric TMD α-indium selenide (In_2Se_3) is one typical representative.

800 Photodetectors based on WSe_2 and α- In_2Se_3 heterostructures have been reported in 2020.

801 [149] and ultra-low dark current of 10^{-13} A was achieved, which is a remarkable result

802 compared to photodetectors with the similar structure. Meanwhile, such device also has high

803 on/off ratio exceeding 1.24×10^5 and photoresponse of 26 mA W^{-1}. Liu *et al.* has also reported

804 InSe2 photodetectors with P(VDF-TrFE) ferroelectric gate. [120] Different polarization of

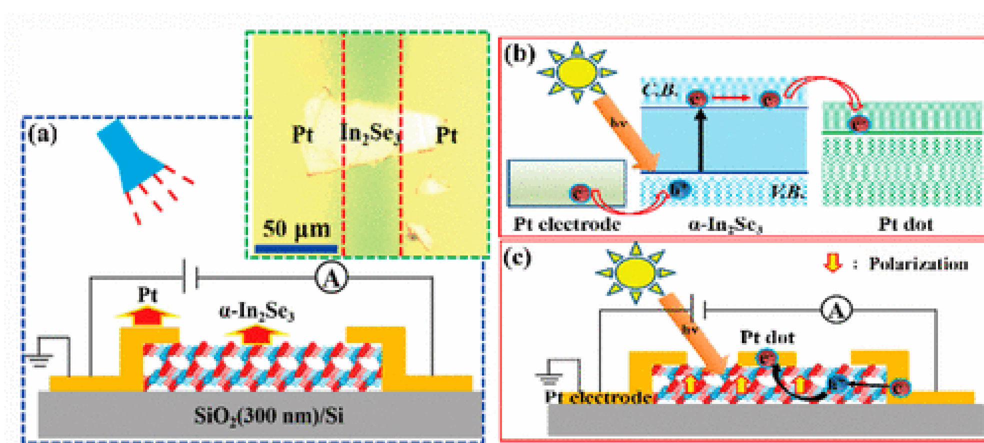

805

806 **Figure 31.** Schematics of the α-In_2Se_3 photodetector.

807 P(VDF-TrFE) was studied to improve the performance of the photodetector. High on/off ratio
808 of 10^8, fast response time of 600 μs and high photoresponsivity up to 14250 AW^{-1} were
809 achieved. However, few researches were focused on the ferroelectricity of InSe materials. Xu
810 et al. as briefly reported the optoelectronic properties in WSe_2/In_2Se_3 heterostructures in 2018,
811 In_2Se_3 was polarized and the output properties in dark and under illumination was investigated,
812 as shown in Figure 32. Photocurrent was enhanced with positive voltage bias applied in gate
813 dielectrics. Enhancement and weaken of the photocurrent were able to be modulated by
814 varying the voltage bias from negative to positive, as shown in Figure 32(f). Photoresponse
815 was thus improved by ferroelectric modulation.

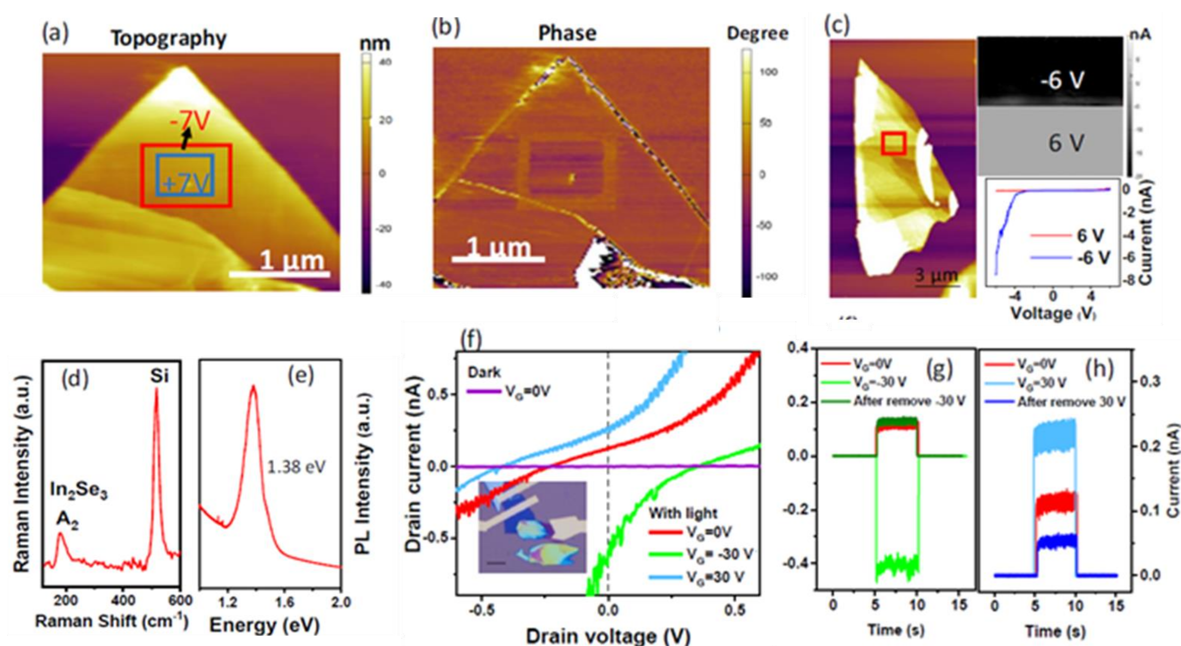

816

817 **Figure 32.** (a) Height image and (b) out-of-plane phase image of In_2Se_3 in PFM measurement.
818 (c) Topography image, current mapping and local IV curves after writing with -6 V and 6 V
819 in CAFM measurement. (d) Raman spectrum and (e) PL spectrum of a α-In_2Se_3 flake. (f)
820 Photocurrent as a function of drain voltage of the photodetector based on WSe_2/In_2Se_3
821 heterostructure measured at various gate voltages. Inset: optical image of the device. (g) and
822 (h) Short-circuit current as a function of time measured in a photodetector based on the
823 WSe_2/In_2Se_3 heterostructure before, during, and after applied +30 V and -30 V gate voltages.

824 **4. Conclusions and perspectives**

825 In this review, we have reviewed the fundamentals of two-dimensional semiconductors and
826 ferroelectrics as well as their application in photodetection. Hybrid system of two-
827 dimensional materials and ferroelectrics could interact with each other, and thus realize higher
828 performances and enable modulation of the devices. This novel combination structure has
829 provided new methods for multiple functional nano-devices and compatible circuits.

830 In materials aspect, structure, physical properties, electrical properties as well as
831 optoelectronic properties has been reviewed. Additionally, interaction between two-
832 dimensional materials and ferroelectrics has been introduced.

833 In devices aspect, photodetectors based on two-dimensional materials and ferroelectrics has
834 been categorized based on their structures and the performances as well as the interaction in
835 the hybrid system has been reviewed. Researches based on two-dimensional materials and
836 ferroelectrics have shown great potential in photodetectors. Remarkable achievements have
837 witnessed however, problems still exit. Considering the structure of the devices, most of the
838 researches focused on the field effect transistors with ferroelectrics as top gate, more work
839 still remains to be done in the study of the ferroelectric layer applied as bottom gate as well as
840 substrates. Meanwhile, photodetectors based on PN junctions are mostly based on the vertical
841 heterojunctions with silicon as substrate or doped lateral junctions. Modulation of the carrier
842 type and the junction generated from ferroelectric polarization has not been fully investigated
843 either. Details and the mechanism of interaction between the two-dimensional semiconductor
844 and the functional ferroelectric layer is still unintelligible, which is currently a challenge for
845 the application of photodetectors based on 2D materials and ferroelectrics. As is mentioned
846 before that the 2D materials has outstanding flexibility and mechanical strength, the joint
847 ferroelectric substrates in the flexible devices are expecting to be flexible and transparent as
848 well. Therefore, more attention is required on designing and fabrication of ultrathin
849 ferroelectric film with high transparency and outstanding mechanical properties.

850 In conclusion, photodetectors based on two dimensional materials, ferroelectrics as well as the
851 hybrid structures is promising structure for wide band high performance photodetection.
852 Ferroelectric provide effective modulation of the devices and thus improve optical and
853 optoelectronic properties of the devices. It is promising that the ferroelectric layer being
854 applied as component of integrated circuit and will certainly lead to another prosperity area in
855 exploring the road "More than Moore".
856

857 **Acknowledgements**
858 We acknowledge the funding support from Key R&D Program of Shaanxi Province of China
859 (2020GY-271 and 2018ZDXM-GY-150), the Fundamental Research Funds for the Central
860 Universities(xjj2018016), the “111 Project” of China (B14040), the Open Project of State Key
861 Laboratory of Infrared Technological Physic (Grant No. M201801), the Open Project of State
862 Key Laboratory of Electronic Thin Films and Integrated Devices (KFJJ201902) and the
863 Natural Sciences and Engineering Research Council of Canada (NSERC DG Grant No.
864 203773).
865

866 Received: ((will be filled in by the editorial staff))
867 Revised: ((will be filled in by the editorial staff))
868 Published online: ((will be filled in by the editorial staff))
869

870 **References**
871 [1] L. Wang, X. Zou, J. Lin, J. Jiang, Y. Liu, X. Liu, X. Zhao, Y. F. Liu, J. C. Ho, L. Liao,
872 *ACS Nano* **2019**, *13*, 4 4804.
873 [2] Z. Yang, L. Liao, F. Gong, F. Wang, Z. Wang, X. Liu, X. Xiao, W. Hu, J. He, X. Duan,
874 *Nano Energy* **2018**, *49* 103 .

875 [3] A. D. Bartolomeo, G. Luongo, F. Giubileo, N. Funicello, G. Niu, T. Schroeder, M.
876 Lisker, G. Lupina, *2D Materials* **2017**, *4*, 2 025075.
877 [4] C. Hu, D. Dong, X. Yang, K. Qiao, D. Yang, H. Deng, S. Yuan, J. Khan, Y. Lan, H.
878 Song, J. Tang, *Advanced Functional Materials* **2017**, *27*, 2 1603605.
879 [5] F. Withers, O. Del Pozo-Zamudio, S. Schwarz, S. Dufferwiel, P. M. Walker, T. Godde,
880 A. P. Rooney, A. Gholinia, C. R. Woods, P. Blake, S. J. Haigh, K. Watanabe, T. Taniguchi, I.
881 L. Aleiner, A. K. Geim, V. I. Fal'ko, A. I. Tartakovskii, K. S. Novoselov, *Nano Lett.* **2015**, *15*,
882 12 8223.
883 [6] F. Withers, O. D. Pozo-Zamudio, A. Mishchenko, A. P. Rooney, A. Gholinia, K.
884 Watanabe, T. Taniguchi, S. J. Haigh, A. K. Geim, A. I. Tartakovskii, K. S. Novoselov, *Nature*
885 *Materials* **2015**, *14*, 3 301.
886 [7] O. Salehzadeh, M. Djavid, N. H. Tran, I. Shih, Z. Mi, *Nano Letters* **2015**, *15*, 8 5302.
887 [8] S. Riechel, C. Kallinger, U. Lemmer, J. Feldmann, A. Gombert, V. Wittwer, U. Scherf,
888 *Applied Physics Letters* **2000**, *77*, 15 2310.
889 [9] G. Wu, X. Wang, P. Wang, H. Huang, Y. Chen, S. Sun, H. Shen, T. Lin, J. Wang, S.
890 Zhang, L. Bian, J. Sun, X. Meng, J. Chu, *Nanotechnology* **2016**, *27*, 36 364002.
891 [10] L. Y. Rang, S. Wooseok, H. J. Kyu, L. Y. Bum, K. S. Jun, M. Sung, L. S. Sook, A. Ki-
892 Seok, C. Chel-Jong, L. Jongsun, *Advanced Materials 28*, 25 5025.
893 [11] N. Huo, S. Gupta, G. Konstantatos, *Advanced Materials* **2017**, *29*, 17 1606576.
894 [12] K. S. Kim, Y. J. Ji, K. H. Kim, S. Choi, D.-H. Kang, K. Heo, S. Cho, S. Yim, S. Lee,
895 J.-H. Park, Y. S. Jung, G. Y. Yeom, *Nature Communications* **2019**, *10*, 1 4701.
896 [13] E. O. Polat, G. Mercier, I. Nikitskiy, E. Puma, T. Galan, S. Gupta, M. Montagut, J. J.
897 Piqueras, M. Bouwens, T. Durduran, G. Konstantatos, S. Goossens, F. Koppens, *Science*
898 *Advances* **2019**, *5*, 9.
899 [14] A. Lipatov, P. Sharma, A. Gruverman, A. Sinitskii, *ACS Nano* **2015**, *9*, 8 8089.

900 [15] D. Xiang, T. Liu, J. Xu, J. Y. Tan, Z. Hu, B. Lei, Y. Zheng, J. Wu, A. H. C. Neto, L.
901 Liu, W. Chen, *Nature Communications* **2018**, *9*, 1.
902 [16] M.-L. Tsai, S.-H. Su, J.-K. Chang, D.-S. Tsai, C.-H. Chen, C.-I. Wu, L.-J. Li, L.-J.
903 Chen, J.-H. He, *ACS Nano* **2014**, *8*, 8 8317.
904 [17] Y. Tsuboi, F. Wang, D. Kozawa, K. Funahashi, S. Mouri, Y. Miyauchi, T. Takenobu,
905 K. Matsuda, *Nanoscale* **2015**, *7*, 34 14476.
906 [18] T. Mueller, F. Xia, P. Avouris, *Nature Photonics* **2010**, *4* 297.
907 [19] Y. Tajima, B. Wrona, K. Mishima, *IEEE Transactions on Electron Devices* **1981**, *28*,
908 2 171.
909 [20] J.-P. Shim, S. K. Kim, H. Kim, G. Ju, H. Lim, S. Kim, H.-j. Kim, *APL Materials* **2018**,
910 *6*, 1 016103.
911 [21] D.-H. Kwak, P. Ramasamy, Y.-S. Lee, M.-H. Jeong, J.-S. Lee, *ACS Appl. Mater.*
912 *Interfaces* **2019**, *11*, 32 29041.
913 [22] A. Levi, M. Kirshner, O. Sinai, E. Peretz, O. Meshulam, A. Ghosh, N. Gotlib, C. Stern,
914 S. Yuan, F. Xia, D. Naveh, *ACS Photonics* **2019**, *6*, 8 1910.
915 [23] C. Xu, Z. Du, Y. Huang, M. Dong, R. Lin, Y. Li, B. Wang, W. Zheng, F. Huang, *ACS*
916 *Appl. Mater. Interfaces* **2018**, *10*, 49 42681.
917 [24] K.-J. Tielrooij, N. C. H. Hesp, A. Principi, M. B. Lundeberg, E. A. A. Pogna, L.
918 Banszerus, Z. Mics, M. Massicotte, P. Schmidt, D. Davydovskaya, D. G. Purdie, I.
919 Goykhman, G. Soavi, A. Lombardo, K. Watanabe, T. Taniguchi, M. Bonn, D. Turchinovich,
920 C. Stampfer, A. C. Ferrari, G. Cerullo, M. Polini, F. H. L. Koppens, *Nature Nanotechnology*
921 **2017**, *13*, 1 41.
922 [25] W. Zheng, R. Lin, J. Ran, Z. Zhang, X. Ji, F. Huang, *ACS Nano* **2018**, *12*, 1 425,
923 pMID: 29298035.
924 [26] P. Ma, Y. Salamin, B. Baeuerle, A. Josten, W. Heni, A. Emboras, J. Leuthold, *ACS*
925 *Photonics* **2019**, *6*, 1 154.

926 [27] K. S. Novoselov, A. K. Geim, S. V. Morozov, D. Jiang, Y. Zhang, S. V. Dubonos, I. V.
927 Grigorieva, A. A. Firsov, *Science* **2004**, *306*, 5696 666.
928 [28] F. Xia, T. Mueller, Y. ming Lin, A. Valdes-Garcia, P. Avouris, *Nature*
929 *Nanotechnology* **2009**, *4*, 12 839.
930 [29] H. Chang, H. Wu, *Advanced Functional Materials* **2012**, *23*, 16 1984.
931 [30] F. Bonaccorso, Z. Sun, T. Hasan, A. C. Ferrari, *Nature Photonics* **2010**, *4*, 9 611.
932 [31] Q. Bao, K. P. Loh, *ACS Nano* **2012**, *6*, 5 3677.
933 [32] H.-Y. Chiu, V. Perebeinos, Y.-M. Lin, P. Avouris, *Nano Letters* **2010**, *10*, 11 4634.
934 [33] S. Castilla, B. Terrés, M. Autore, L. Viti, J. Li, A. Y. Nikitin, I. Vangelidis, K.
935 Watanabe, T. Taniguchi, E. Lidorikis, M. S. Vitiello, R. Hillenbrand, K.-J. Tielrooij, F. H.
936 Koppens, *Nano Letters* **2019**, *19*, 5 2765.
937 [34] K. S. Novoselov, A. Mishchenko, A. Carvalho, A. H. C. Neto, *Science* **2016**, *353*,
938 6298 aac9439.
939 [35] A. Gupta, T. Sakthivel, S. Seal, *Progress in Materials Science* **2015**, *73* 44.
940 [36] X. Li, L. Tao, Z. Chen, H. Fang, X. Li, X. Wang, J.-B. Xu, H. Zhu, *Applied Physics*
941 *Reviews* **2017**, *4*, 2 021306.
942 [37] X. Yao, Y. Wang, X. Lang, Y. Zhu, Q. Jiang, *Physica E: Low-dimensional Systems*
943 *and Nanostructures* **2019**, *109* 11.
944 [38] X.-L. Li, W.-P. Han, J.-B. Wu, X.-F. Qiao, J. Zhang, P.-H. Tan, *Advanced Functional*
945 *Materials* **2017**, *27*, 19 1604468.
946 [39] I. Husein, R. P. Jenie, In *Ferroelectrics and Their Applications*. InTech, **2018**.
947 [40] Y. Zhang, W. Jie, P. Chen, W. Liu, J. Hao, *Advanced Materials* **2018**, *30*, 34 1707007.
948 [41] L. Li, X. Liu, Y. Li, Z. Xu, Z. Wu, S. Han, K. Tao, M. Hong, J. Luo, Z. Sun, *Journal*
949 *of the American Chemical Society* **2019**, *141*, 6 2623, pMID: 30661350.
950 [42] Y. Yuan, Z. Xiao, B. Yang, J. Huang, *J. Mater. Chem. A* **2014**, *2*, 17 6027.

951 [43] A. Lipatov, T. Li, N. S. Vorobeva, A. Sinitskii, A. Gruverman, *Nano Letters* **2019**, *19*,
952 5 3194.
953 [44] J. Íñiguez, P. Zubko, I. Luk'yanchuk, A. Cano, *Nature Reviews Materials* **2019**, *4*, 4
954 243.
955 [45] G. Wu, X. Wang, Y. Chen, S. Wu, B. Wu, Y. Jiang, H. Shen, T. Lin, Q. Liu, X. Wang,
956 P. Zhou, S. Zhang, W. Hu, X. Meng, J. Chu, J. Wang, *Advanced Materials* **2020**, *32*, 16
957 1907937.
958 [46] C. A. Randall, D. J. Barber, R. W. Whatmore, *Journal of Materials Science* **1987**, *22*,
959 3 925.
960 [47] Z. Surowiak, M. Kupriyanov, D. Czekaj, *Journal of the European Ceramic Society*
961 **2001**, *21*, 10-11 1377.
962 [48] K. Kushida-Abdelghafar, H. Miki, K. Torii, Y. Fujisaki, *Applied Physics Letters* **1996**,
963 *69*, 21 3188.
964 [49] R. Moazzami, C. Hu, W. H. Shepherd, *IEEE Transactions on Electron Devices* **1992**,
965 *39*, 9 2044.
966 [50] B. Ravel, E. A. Stern, R. I. Vedrinskii, V. Kraizman, *Ferroelectrics* **1998**, *206*, 1 407.
967 [51] C. Xiong, W. H. P. Pernice, J. H. Ngai, J. W. Reiner, D. Kumah, F. J. Walker, C. H.
968 Ahn, H. X. Tang, *Nano Letters* **2014**, *14*, 3 1419.
969 [52] E. Strelcov, A. V. Ievlev, S. Jesse, I. I. Kravchenko, V. Y. Shur, S. V. Kalinin,
970 *Advanced Materials* **2013**, *26*, 6 958.
971 [53] A. Kuroda, S. Kurimura, Y. Uesu, *Applied Physics Letters* **1996**, *69*, 11 1565.
972 [54] K. Y. Yun, M. Noda, M. Okuyama, *Applied Physics Letters* **2003**, *83*, 19 3981.
973 [55] T. Choi, S. Lee, Y. J. Choi, V. Kiryukhin, S.-W. Cheong, *Science* **2009**, *324*, 5923 63.
974 [56] G. D. Hu, S. H. Fan, C. H. Yang, W. B. Wu, *Applied Physics Letters* **2008**, *92*, 19
975 192905.

976 [57] S. Trolier-McKinstry, C. A. Randall, *Journal of the American Ceramic Society* **2017**,
977 *100*, 8 3346.
978 [58] M. Sharma, G. Madras, S. Bose, *Physical Chemistry Chemical Physics* **2014**, *16*, 28
979 14792.
980 [59] S. Lee, Y. Lee, *Carbon* **2018**, *126* 176.
981 [60] W. Ren, Y. Fang, E. Wang, *ACS Nano* **2011**, *5*, 8 6425.
982 [61] D. A. Hon-Sum Philip Wong, *Carbon Nanotube and Graphene Device Physics*,
983 Cambridge University Press, **2014**.
984 [62] S. Reich, J. Maultzsch, C. Thomsen, P. Ordejón, *Physical Review B* **2002**, *66*, 3.
985 [63] G. Gui, J. Li, J. Zhong, *Physical Review B* **2008**, *78*, 7.
986 [64] M. Gmitra, S. Konschuh, C. Ertler, C. Ambrosch-Draxl, J. Fabian, *Phys. Rev. B* **2009**,
987 *80* 235431.
988 [65] J.-H. Chen, W. G. Cullen, C. Jang, M. S. Fuhrer, E. D. Williams, *Physical Review*
989 *Letters* **2009**, *102*, 23.
990 [66] K. Bolotin, K. Sikes, Z. Jiang, M. Klima, G. Fudenberg, J. Hone, P. Kim, H. Stormer,
991 *Solid State Communications* **2008**, *146*, 9-10 351.
992 [67] F. Schwierz, *Nature Nanotechnology* **2010**, *5*, 7 487.
993 [68] J. Yu, G. Liu, A. V. Sumant, V. Goyal, A. A. Balandin, *Nano Letters* **2012**, *12*, 3 1603.
994 [69] K. Zhao, T. Zhang, A. Ren, Y. Yang, P. Xiao, Z. Ge, Y. Ma, Y. Chen, *Carbon* **2019**,
995 *141* 198.
996 [70] T. Yu, E.-K. Lee, B. Briggs, B. Nagabhirava, B. Yu, *IEEE Electron Device Letters*
997 **2010**, *31*, 10 1155.
998 [71] A. A. Balandin, S. Ghosh, W. Bao, I. Calizo, D. Teweldebrhan, F. Miao, C. N. Lau,
999 *Nano Letters* **2008**, *8*, 3 902.

1000 [72] J. S. Moon, M. Antcliffe, H. C. Seo, D. Curtis, S. Lin, A. Schmitz, I. Milosavljevic, A.
1001 A. Kiselev, R. S. Ross, D. K. Gaskill, P. M. Campbell, R. C. Fitch, K.-M. Lee, P. Asbeck,
1002 *Applied Physics Letters* **2012**, *100*, 20 203512.
1003 [73] G. Lu, K. Yu, Z. Wen, J. Chen, *Nanoscale* **2013**, *5*, 4 1353.
1004 [74] M. F. Craciun, S. Russo, M. Yamamoto, J. B. Oostinga, A. F. Morpurgo, S. Tarucha,
1005 *Nature Nanotechnology* **2009**, *4*, 6 383.
1006 [75] O. V. Gamayun, E. V. Gorbar, V. P. Gusynin, *Physical Review B* **2010**, *81*, 7.
1007 [76] X. Yang, G. Liu, M. Rostami, A. A. Balandin, K. Mohanram, *IEEE Electron Device*
1008 *Letters* **2011**, *32*, 10 1328.
1009 [77] H. Li, Q. Zhang, C. Liu, S. Xu, P. Gao, *ACS Nano* **2011**, *5*, 4 3198.
1010 [78] J. F. Tian, L. A. Jauregui, G. Lopez, H. Cao, Y. P. Chen, *Applied Physics Letters* **2010**,
1011 *96*, 26 263110.
1012 [79] B. Y. Zhang, T. Liu, B. Meng, X. Li, G. Liang, X. Hu, Q. J. Wang, *Nature*
1013 *Communications* **2013**, *4*, 1.
1014 [80] A. Pospischil, M. Humer, M. M. Furchi, D. Bachmann, R. Guider, T. Fromherz, T.
1015 Mueller, *Nature Photonics* **2013**, *7*, 11 892.
1016 [81] M. Liu, X. Yin, E. Ulin-Avila, B. Geng, T. Zentgraf, L. Ju, F. Wang, X. Zhang, *Nature*
1017 **2011**, *474*, 7349 64.
1018 [82] S. Cho, M. S. Fuhrer, *Physical Review B* **2008**, *77*, 8.
1019 [83] F. Wang, Y. Zhang, C. Tian, C. Girit, A. Zettl, M. Crommie, Y. R. Shen, *Science* **2008**,
1020 *320*, 5873 206.
1021 [84] J. M. Dawlaty, S. Shivaraman, J. Strait, P. George, M. Chandrashekhar, F. Rana, M. G.
1022 Spencer, D. Veksler, Y. Chen, *Applied Physics Letters* **2008**, *93*, 13 131905.
1023 [85] K. F. Mak, M. Y. Sfeir, Y. Wu, C. H. Lui, J. A. Misewich, T. F. Heinz, *Physical*
1024 *Review Letters* **2008**, *101*, 19.
1025 [86] G. Xing, H. Guo, X. Zhang, T. C. Sum, C. H. A. Huan, *Opt. Express* **2010**, *18*, 5 4564.

1026 [87] H. Yang, X. Feng, Q. Wang, H. Huang, W. Chen, A. T. S. Wee, W. Ji, *Nano Letters*
1027 **2011**, *11*, 7 2622.
1028 [88] G.-K. Lim, Z.-L. Chen, J. Clark, R. G. S. Goh, W.-H. Ng, H.-W. Tan, R. H. Friend, P.
1029 K. H. Ho, L.-L. Chua, *Nature Photonics* **2011**, *5*, 9 554.
1030 [89] E. H. Hwang, S. D. Sarma, *Physical Review B* **2007**, *75*, 20.
1031 [90] A. N. Grigorenko, M. Polini, K. S. Novoselov, *Nature Photonics* **2012**, *6*, 11 749.
1032 [91] D. Voiry, A. Mohite, M. Chhowalla, *Chemical Society Reviews* **2015**, *44*, 9 2702.
1033 [92] X. Fan, P. Xu, D. Zhou, Y. Sun, Y. C. Li, M. A. T. Nguyen, M. Terrones, T. E.
1034 Mallouk, *Nano Letters* **2015**, *15*, 9 5956.
1035 [93] F. Wypych, R. Schollhorn, *J. Chem. Soc., Chem. Commun.* **1992**, , 19 1386.
1036 [94] R. Ganatra, Q. Zhang, *ACS Nano* **2014**, *8*, 5 4074.
1037 [95] C. Huang, S. Wu, A. M. Sanchez, J. J. P. Peters, R. Beanland, J. S. Ross, P. Rivera, W.
1038 Yao, D. H. Cobden, X. Xu, *Nature Materials* **2014**, *13*, 12 1096.
1039 [96] C. Cong, J. Shang, X. Wu, B. Cao, N. Peimyoo, C. Qiu, L. Sun, T. Yu, *Advanced*
1040 *Optical Materials* **2013**, *2*, 2 131.
1041 [97] Y. Zhang, L. Yin, J. Chu, T. A. Shifa, J. Xia, F. Wang, Y. Wen, X. Zhan, Z. Wang, J.
1042 He, *Advanced Materials* **2018**, *30*, 40 1803665.
1043 [98] A. Splendiani, L. Sun, Y. Zhang, T. Li, J. Kim, C.-Y. Chim, G. Galli, F. Wang, *Nano*
1044 *Letters* **2010**, *10*, 4 1271.
1045 [99] Y. Yu, J. Yao, X. Niu, B. Xing, Y. Liu, X. Wu, M. Li, X. Yan, J. Sha, Y. Wang,
1046 *CrystEngComm* **2020**, *22*, 22 3824.
1047 [100] J. Miao, L. Zhang, C. Wang, *2D Materials* **2019**, *6*, 3 032003.
1048 [101] Y. Yi, Z. Sun, J. Li, P. K. Chu, X.-F. Yu, *Small Methods* **2019**, *3*, 10 1900165.
1049 [102] S. Pandey, A. James, R. Raman, S. Chatterjee, A. Goyal, C. Prakash, T. Goel, *Physica*
1050 *B: Condensed Matter* **2005**, *369*, 1-4 135.

1051 [103] G. Kwei, A. Lawson, S. Billinge, S.-W. Cheong, *The Journal of Physical Chemistry*
1052 **1993**, *97*, 10 2368.
1053 [104] M. Klee, R. Mauczok, C. V. Heesch, B. op het Veld, M. D. Wild, H. Boots, B. Kumar,
1054 W. Soer, G. Schmitz, M. Mleczko, *Integrated Ferroelectrics* **2012**, *134*, 1 25.
1055 [105] T. Gu, T. Scarbrough, Y. Yang, J. Íñiguez, L. Bellaiche, H. J. Xiang, *Phys. Rev. Lett.*
1056 **2018**, *120* 197602.
1057 [106] N. Setter, D. Damjanovic, L. Eng, G. Fox, S. Gevorgian, S. Hong, A. Kingon, H.
1058 Kohlstedt, N. Y. Park, G. B. Stephenson, I. Stolitchnov, A. K. Taganstev, D. V. Taylor, T.
1059 Yamada, S. Streiffer, *Journal of Applied Physics* **2006**, *100*, 5 051606.
1060 [107] O. I. Prokopalo, A. V. Turik, *Ferroelectrics* **1978**, *22*, 1 749.
1061 [108] J. Jiang, Y. Bitla, C.-W. Huang, T. H. Do, H.-J. Liu, Y.-H. Hsieh, C.-H. Ma, C.-Y.
1062 Jang, Y.-H. Lai, P.-W. Chiu, W.-W. Wu, Y.-C. Chen, Y.-C. Zhou, Y.-H. Chu, *Science*
1063 *Advances* **2017**, *3*, 6 e1700121.
1064 [109] D. Páez-Margarit, F. Rubio-Marcos, D. A. Ochoa, A. D. Campo, J. F. Fernández, J. E.
1065 Garcá, *ACS Applied Materials & Interfaces* **2018**, *10*, 26 21804.
1066 [110] A. Boes, T. Crasto, H. Steigerwald, S. Wade, J. Frohnhaus, E. Soergel, A. Mitchell,
1067 *Applied Physics Letters* **2013**, *103*, 14 142904.
1068 [111] H. Steigerwald, Y. J. Ying, R. W. Eason, K. Buse, S. Mailis, E. Soergel, *Applied*
1069 *Physics Letters* **2011**, *98*, 6 062902.
1070 [112] P. J. Sturman, *Photovoltaic and Photo-refractive Effects in Noncentrosymmetric*
1071 *Materials*, volume 8, CRC Press, **1992**.
1072 [113] T. Li, A. Lipatov, H. Lu, H. Lee, J.-W. Lee, E. Torun, L. Wirtz, C.-B. Eom, J. Íñiguez,
1073 A. Sinitskii, A. Gruverman, *Nature Communications* **2018**, *9*, 1.
1074 [114] M.-M. Yang, M. Alexe, *Advanced Materials* **2018**, *30*, 14 1704908.
1075 [115] H. J. Lee, J. Kim, O. Kwon, H. J. Lee, J. H. Kwak, J. M. Kim, S. S. Lee, Y. Kim, D.-Y.
1076 Kim, J. Y. Jo, *Applied Physics Letters* **2015**, *107*, 26 262902.

1077 [116] Y. Sun, D. Xie, X. Zhang, J. Xu, X. Li, X. Li, R. Dai, X. Li, P. Li, X. Gao, H. Zhu,
1078 *Nanotechnology* **2016**, *28*, 4 045204.
1079 [117] W. Kim, A. Javey, O. Vermesh, Q. Wang, Y. Li, H. Dai, *Nano Letters* **2003**, *3*, 2 193.
1080 [118] J. S. Lee, S. Ryu, K. Yoo, I. S. Choi, W. S. Yun, J. Kim, *The Journal of Physical*
1081 *Chemistry C* **2007**, *111*, 34 12504.
1082 [119] J. Jiang, X. Zou, Y. Lv, Y. Liu, W. Xu, Q. Tao, Y. Chai, L. Liao, *Nature*
1083 *Communications* **2020**, *11*, 1.
1084 [120] L. Liu, L. Wu, A. Wang, H. Liu, R. Ma, K. Wu, J. Chen, Z. Zhou, Y. Tian, H. Yang, C.
1085 Shen, L. Bao, Z. Qin, S. T. Pantelides, H.-J. Gao, *Nano Letters* **2020**, *20*, 9 6666.
1086 [121] A. Lipatov, A. Fursina, T. H. Vo, P. Sharma, A. Gruverman, A. Sinitskii, *Advanced*
1087 *Electronic Materials* **2017**, *3*, 7 1700020.
1088 [122] L. Lv, F. Zhuge, F. Xie, X. Xiong, Q. Zhang, N. Zhang, Y. Huang, T. Zhai, *Nature*
1089 *Communications* **2019**, *10*, 1.
1090 [123] C. Baeumer, S. P. Rogers, R. Xu, L. W. Martin, M. Shim, *Nano Letters* **2013**, *13*, 4
1091 1693, pMID: 23506048.
1092 [124] J. Li, Z. Wang, Y. Wen, J. Chu, L. Yin, R. Cheng, L. Lei, P. He, C. Jiang, L. Feng, J.
1093 He, *Advanced Functional Materials* **2018**, *28*, 10 1706437.
1094 [125] A. Nguyen, P. Sharma, T. Scott, E. Preciado, V. Klee, D. Sun, I.-H. D. Lu, D. Barroso,
1095 S. Kim, V. Y. Shur, A. R. Akhmatkhanov, A. Gruverman, L. Bartels, P. A. Dowben, *Nano*
1096 *Letters* **2015**, *15*, 5 3364.
1097 [126] C. H. Li, K. M. McCreary, B. T. Jonker, *ACS Omega* **2016**, *1*, 6 1075.
1098 [127] C. Baeumer, D. Saldana-Greco, J. M. P. Martirez, A. M. Rappe, M. Shim, L. W.
1099 Martin, *Nature Communications* **2015**, *6*, 1.
1100 [128] M. ukaszewicz, P. Guchowski, B. Cichy, W. Strek, *Physics Procedia* **2015**, *76* 155.
1101 [129] Z. Yin, H. Li, H. Li, L. Jiang, Y. Shi, Y. Sun, G. Lu, Q. Zhang, X. Chen, H. Zhang,
1102 *ACS Nano* **2011**, *6*, 1 74.

1103 [130] J. Wang, H. Fang, X. Wang, X. Chen, W. Lu, W. Hu, *Small* **2017**, *13*, 35 1700894.

1104 [131] P. L. Richards, *Journal of Applied Physics* **1994**, *76*, 1 1.

1105 [132] N. M. Gabor, J. C. W. Song, Q. Ma, N. L. Nair, T. Taychatanapat, K. Watanabe, T.
1106 Taniguchi, L. S. Levitov, P. Jarillo-Herrero, *Science* **2011**, *334*, 6056 648.

1107 [133] N. Huo, G. Konstantatos, *Nature Communications* **2017**, *8*, 1.

1108 [134] J. Chi, N. Guo, Y. Sun, G. Li, L. Xiao, *Nanoscale Research Letters* **2020**, *15*, 1.

1109 [135] F. H. L. Koppens, T. Mueller, P. Avouris, A. C. Ferrari, M. S. Vitiello, M. Polini,
1110 *Nature Nanotechnology* **2014**, *9*, 10 780.

1111 [136] R. Zhuo, L. Zeng, H. Yuan, D. Wu, Y. Wang, Z. Shi, T. Xu, Y. Tian, X. Li, Y. H.
1112 Tsang, *Nano Research* **2018**, *12*, 1 183.

1113 [137] Y. Liu, J. Wang, H. Huang, Y. Yun, D. Meng, Q. Yang, X. Zhai, Z. Fu, R. J. Knize, Y.
1114 Lu, *Advanced Optical Materials* **2017**, *5*, 12 1700158.

1115 [138] E. J. H. Lee, K. Balasubramanian, R. T. Weitz, M. Burghard, K. Kern, *Nature*
1116 *Nanotechnology* **2008**, *3*, 8 486.

1117 [139] K. S. Novoselov, D. Jiang, F. Schedin, T. J. Booth, V. V. Khotkevich, S. V. Morozov,
1118 A. K. Geim, *Proceedings of the National Academy of Sciences* **2005**, *102*, 30 10451.

1119 [140] C. Zhou, X. Wang, S. Raju, Z. Lin, D. Villaroman, B. Huang, H. L.-W. Chan, M.
1120 Chan, Y. Chai, *Nanoscale* **2015**, *7*, 19 8695.

1121 [141] G. Rao, X. Wang, Y. Wang, P. Wangyang, C. Yan, J. Chu, L. Xue, C. Gong, J. Huang,
1122 J. Xiong, Y. Li, *InfoMat* **2019**, *1*, 3 272.

1123 [142] X. Wang, P. Wang, J. Wang, W. Hu, X. Zhou, N. Guo, H. Huang, S. Sun, H. Shen, T.
1124 Lin, M. Tang, L. Liao, A. Jiang, J. Sun, X. Meng, X. Chen, W. Lu, J. Chu, *Advanced*
1125 *Materials* **2015**, *27*, 42 6538.

1126 [143] Y. Chen, X. Wang, P. Wang, H. Huang, G. Wu, B. Tian, Z. Hong, Y. Wang, S. Sun, H.
1127 Shen, J. Wang, W. Hu, J. Sun, X. Meng, J. Chu, *ACS Appl. Mater. Interfaces* **2016**, *8*, 47
1128 32083.

1129 [144] W. Wu, D. De, S.-C. Chang, Y. Wang, H. Peng, J. Bao, S.-S. Pei, *Applied Physics*
1130 *Letters* **2013**, *102*, 14 142106.
1131 [145] X. Tong, E. Ashalley, F. Lin, H. Li, Z. M. Wang, *Nano-Micro Letters* **2015**, *7*, 3 203.
1132 [146] S. Wu, G. Wu, X. Wang, Y. Chen, T. Lin, H. Shen, W. Hu, X. Meng, J. Wang, J. Chu,
1133 *Journal of Semiconductors* **2019**, *40*, 9 092002.
1134 [147] J. Guo, S. Li, Y. Ke, L. Mao, W. Huang, X. Zhang, In H. Wang, editor, *Eleventh*
1135 *International Conference on Information Optics and Photonics (CIOP 2019)*. SPIE, **2019** .
1136 [148] P. Hou, Y. Lv, X. Zhong, J. Wang, *ACS Applied Nano Materials* **2019**, *2*, 7 4443.
1137 [149] B. Liu, B. Tang, F. Lv, Y. Zeng, J. Liao, S. Wang, Q. Chen, *Nanotechnology* **2019**, *31*,
1138 6 065203.
1139 [150] G. L. Frey, S. Elani, M. Homyonfer, Y. Feldman, R. Tenne, *Physical Review B* **1998**,
1140 *57*, 11 6666.
1141 [151] G. Cunningham, D. Hanlon, N. McEvoy, G. S. Duesberg, J. N. Coleman, *Nanoscale*
1142 **2015**, *7*, 1 198.
1143 [152] K. F. Mak, C. Lee, J. Hone, J. Shan, T. F. Heinz, *Physical Review Letters* **2010**, *105*,
1144 13.
1145 [153] K. K. Kam, B. A. Parkinson, *The Journal of Physical Chemistry* **1982**, *86*, 4 463.
1146 [154] S. Tongay, J. Zhou, C. Ataca, K. Lo, T. S. Matthews, J. Li, J. C. Grossman, J. Wu,
1147 *Nano Letters* **2012**, *12*, 11 5576.
1148 [155] Y. Ma, Y. Dai, M. Guo, C. Niu, J. Lu, B. Huang, *Physical Chemistry Chemical*
1149 *Physics* **2011**, *13*, 34 15546.
1150 [156] W. Li, T. Wang, X. Dai, X. Wang, C. Zhai, Y. Ma, S. Chang, *Solid State*
1151 *Communications* **2016**, *225* 32.
1152 [157] H. R. Gutiérrez, N. Perea-López, A. L. Elás, A. Berkdemir, B. Wang, R. Lv, F. López-
1153 Urás, V. H. Crespi, H. Terrones, M. Terrones, *Nano Letters* **2012**, *13*, 8 3447.
1154 [158] A. Kuc, N. Zibouche, T. Heine, *Physical Review B* **2011**, *83*, 24.

1155 [159] S. B. Desai, G. Seol, J. S. Kang, H. Fang, C. Battaglia, R. Kapadia, J. W. Ager, J. Guo,
1156 A. Javey, *Nano Letters* **2014**, *14*, 8 4592.
1157 [160] L. Brixner, *Journal of Inorganic and Nuclear Chemistry* **1962**, *24*, 3 257.
1158 [161] W. S. Yun, S. W. Han, S. C. Hong, I. G. Kim, J. D. Lee, *Physical Review B* **2012**, *85*,
1159 3.
1160 [162] D. H. Keum, S. Cho, J. H. Kim, D.-H. Choe, H.-J. Sung, M. Kan, H. Kang, J.-Y.
1161 Hwang, S. W. Kim, H. Yang, K. J. Chang, Y. H. Lee, *Nature Physics* **2015**, *11*, 6 482.
1162 [163] Y.-F. Lin, Y. Xu, S.-T. Wang, S.-L. Li, M. Yamamoto, A. Aparecido-Ferreira, W. Li,
1163 H. Sun, S. Nakaharai, W.-B. Jian, K. Ueno, K. Tsukagoshi, *Advanced Materials* **2014**, *26*, 20
1164 3263.
1165 [164] I. G. Lezama, A. Arora, A. Ubaldini, C. Barreteau, E. Giannini, M. Potemski, A. F.
1166 Morpurgo, *Nano Letters* **2015**, *15*, 4 2336.
1167 [165] C. Ruppert, O. B. Aslan, T. F. Heinz, *Nano Letters* **2014**, *14*, 11 6231.
1168 [166] A. Kumar, P. K. Ahluwalia, *The European Physical Journal B* **2012**, *85*, 6.
1169 [167] C.-H. Lee, E. C. Silva, L. Calderin, M. A. T. Nguyen, M. J. Hollander, B. Bersch, T. E.
1170 Mallouk, J. A. Robinson, *Scientific Reports* **2015**, *5*, 1.
1171 [168] D. Mao, B. Du, D. Yang, S. Zhang, Y. Wang, W. Zhang, X. She, H. Cheng, H. Zeng, J.
1172 Zhao, *Small* **2016**, *12*, 11 1489.
1173 [169] S. Samanta, M. Rath, V. Sankaranarayanan, K. Sethupathi, M. S. R. Rao, *physica*
1174 *status solidi (b)* **2019**, *257*, 1 1900272.
1175 [170] Y. H. Paik, H. S. Kojori, J.-H. Yun, S. J. Kim, *Materials Letters* **2016**, *185* 247.
1176 [171] M. Zhu, Z. Du, H. Li, B. Chen, L. Jing, R. Y. J. Tay, J. Lin, S. H. Tsang, E. H. T. Teo,
1177 *Applied Surface Science* **2017**, *425* 1059.
1178 [172] R. S. Ganesh, S. K. Sharma, N. Abinnas, E. Durgadevi, P. Raji, S. Ponnusamy, C.
1179 Muthamizhchelvan, Y. Hayakawa, D. Y. Kim, *Materials Chemistry and Physics* **2017**, *192*
1180 274.

1181 [173] D. Sando, C. Carrétéro, M. N. Grisolia, A. Barthélémy, V. Nagarajan, M. Bibes,
1182 *Advanced Optical Materials* **2017**, *6*, 2 1700836.
1183 [174] L. Qiao, S. Zhang, H. Y. Xiao, D. J. Singh, K. H. L. Zhang, Z. J. Liu, X. T. Zu, S. Li,
1184 *Journal of Materials Chemistry C* **2018**, *6*, 5 1239.
1185 [175] T. Onaya, T. Nabatame, N. Sawamoto, A. Ohi, N. Ikeda, T. Nagata, A. Ogura,
1186 *Microelectronic Engineering* **2019**, *215* 111013.